UHASSELT
KNOWLEDGE IN ACTION

Maastricht University

Faculty of Medicine and Life Sciences
School for Life Sciences
Master of Biomedical Sciences

Master's thesis

Investigating the relationship between the actin-spectrin periodic scaffold and clathrin-mediated endocytosis at the axon initial segment

Eline Simons

Thesis presented in fulfillment of the requirements for the degree of Master of Biomedical Sciences, specialization Molecular Mechanisms in Health and Disease

SUPERVISOR :

Prof. dr. Niels HELLINGS

SUPERVISOR :

Prof. Christophe LETERRIER

2023
2024

Transnational University Limburg is a unique collaboration of two universities in two countries: the University of Hasselt and Maastricht University.

UHASSELT
KNOWLEDGE IN ACTION

www.uhasselt.be
Universiteit Hasselt
Campus Hasselt:
Martelarenlaan 42 | 3500 Hasselt
Campus Diepenbeek:
Agoralaan Gebouw D | 3590 Diepenbeek

Maastricht University

Faculty of Medicine and Life Sciences
School for Life Sciences
Master of Biomedical Sciences

Master's thesis

Investigating the relationship between the actin-spectrin periodic scaffold and clathrin-mediated endocytosis at the axon initial segment

Eline Simons

Thesis presented in fulfillment of the requirements for the degree of Master of Biomedical Sciences, specialization Molecular Mechanisms in Health and Disease

SUPERVISOR :

Prof. dr. Niels HELLINGS

SUPERVISOR :

Prof. Christophe LETERRIER

Investigating the relationship between the actin-spectrin periodic scaffold and clathrin-mediated endocytosis at the axon initial segment

Eline Simons[1], Florian Wernert[1], Fanny Boroni-Rueda[1], Florence Pelletier[1], Marie-Jeanne Papandréou[1], Christophe Leterrier[1]

[1]Neurocytolab, Institut de Neurophysiopathologie (INP), Aix-Marseille Université, 27 Bd Jean Moulin, 13005 Marseille, FRANCE

*Running title: *Endocytosis along the proximal axon*

To whom correspondence should be addressed: Dr. Christophe Leterrier, Email: christophe.leterrier@univ-amu.fr

Keywords: axonal initial segment, actin rings, spectrin, membrane-associated period scaffold (MPS), clathrin, clathrin-mediated endocytosis

ABSTRACT

Neuronal cells heavily rely on clathrin-mediated endocytosis. This process is mainly studied in somatodendritic compartments and at presynapses. However, this mechanism is poorly studied along the axon shaft. It has recently been shown by our lab that the surface of the proximal axon is studded with clathrin-coated pits encased in circular clearings of a submembranous structure. This submembranous structure called the membrane-associated periodic scaffold (MPS), is made up of actin rings connected by a spectrin mesh. Endocytosis along the axon is nevertheless a rare event as the clearing-encased pits are stably stalled at the membrane. Endocytosis can be triggered by stimuli such as elevated neuronal activity induced by NMDA.

In this research project, we used super-resolution microscopy techniques in combination with uptake assays and MPS-modulating drugs to investigate the underlying mechanism that drives clathrin-mediated endocytosis along the proximal axon of cultured embryonic rat hippocampal neurons. Results have shown partial disruption of the spectrin scaffold and increased clathrin-mediated endocytosis after NMDA-induced long-term depression. Furthermore, we observed actin polymerization around clathrin pits after NMDA treatment, and preventing this polymerization with latrunculin A inhibited the increase in endocytosis. This suggests that actin polymerization triggers endocytosis from stalled pits along the axon, driving the endocytosis of membrane proteins such as ion channels.

This newly discovered "ready-to-go" endocytic mechanism along the axon offers us new insights into the functions of the axonal MPS and might lead to new understandings of neurodegenerative diseases.

INTRODUCTION

Trillions of axonal connections in the brain enable neurons to communicate with each other and establish intricate networks (1). The axon is an essential part of the neuron that transports important cellular information to a multitude of cell types by transforming chemical input into electrical currents. In neurodegenerative diseases such as Alzheimer's and Parkinson's disease, the axon is usually the first target of degeneration, resulting in less efficient information transfer (2). Understanding this key neuronal compartment is therefore essential to unravel underlying molecular mechanisms in neurological diseases.

The axon can be separated into two main compartments that vary in their molecular composition: the proximal and distal axon. The proximal axon houses a unique area separating the neuronal soma from the beginning of the axon termed the axonal initial segment (AIS). The AIS makes up the first 20-40 µm of the axon and has a specialized function in generating action potentials (3, 4). The central role of the AIS in initiating action potentials is reflected in the high density of Na^+ and K^+ channels tightly anchored to the scaffolding protein ankyrin G along its plasma membrane (5, 6). Furthermore, the AIS is also found to be essential in maintaining axonal polarity (4).

The proximal and distal axons are both supported by a distinct submembranous organization of actin rings regularly interspaced every 190 nm with spectrin tetramers **(figure 1)** (7). The 190 nm distance between the actin rings corresponds to the length of the spectrin tetramers which are organized in a head-to-head manner **(figure 1)** (7). The entirety of this structure is called the membrane-associated periodic scaffold (MPS) and was observed for the first time in hippocampal neurons of the rat using super-resolution microscopy (7). The periodic structure of the MPS remained unobserved for a long time due to the inability of conventional microscopes to resolve the ~190 nm periodicity, which is below the diffraction limit of light (8). Based on the location of the MPS in the axon, the spectrin tetramers vary in their composition; the AIS is made up of α2/β4 spectrin tetramers **(figure 1A)**, while the most distal parts of the axon contain α2/β2 spectrin tetramers **(figure 1B)** (8, 9). This makes it possible to distinguish axonal compartments based on the difference in β-spectrin isoforms. The physiological importance of this unique cytoskeletal organization consists of maintaining axonal structure and robustness to withstand the high amount of mechanical stress that the axon is constantly exposed to (8, 10). Besides its mechanically supportive function, emerging evidence also strongly indicates the regulating effect on endocytosis along the axonal shaft (11). Since its discovery in 1964, clathrin-mediated endocytosis (CME) is the most studied and major endocytic pathway used by eukaryotic cells to sort and internalize extracellular components or cell-surface receptors (12, 13). For CME to occur, clathrin-coated pits (CCPs) form at the bare plasma membrane. These diffraction-limited structures are made up of clathrin triskelia composed of three clathrin heavy chains and three clathrin light chains (14, 15). The clathrin triskelia self-assemble together with adaptor proteins to form ~100 nm polyhedral lattices covering invaginations of the cellular plasma membrane, which gives them their characteristic honeycomb-like appearance (14-16). At the level of the central nervous system, endocytosis is well-defined at synaptic and dendritic sites, while there is still a lack of understanding of endocytosis along axons (11, 17). Existing research primarily looks at the importance of CME in the axon outgrowth of developing axons (18-21). Recently, it was shown by diffraction-limited microscopy that CME is important in the maintenance of neuronal polarity at the AIS by removing and degrading polarized transmembrane proteins (22). Owing to the advancement of microscopy techniques, the first nanoscopic observations of CCPs along the AIS were made by Wernert, Moparthi *et al.* (11). Despite CCPs being present along the AIS, additional research by our team has shown that these pits are mostly stationary (11). Furthermore, the pits have been revealed to be exclusively residing in ~300 nm clearings of the axonal MPS by platinum replica electron microscopy (PREM) (11). Wernert Moparthi *et al.* also observed that when more clearings are introduced by perturbing the MPS with for example diamide, a spectrin-perturbing drug, CCP formation increases (11). This finding leads to the emergence of a new function of the MPS acting as a barrier impeding CCP formation along the axon **(figure 1A-B)** (11). Moreover, they showed that CME could be triggered after physiologically stimulating

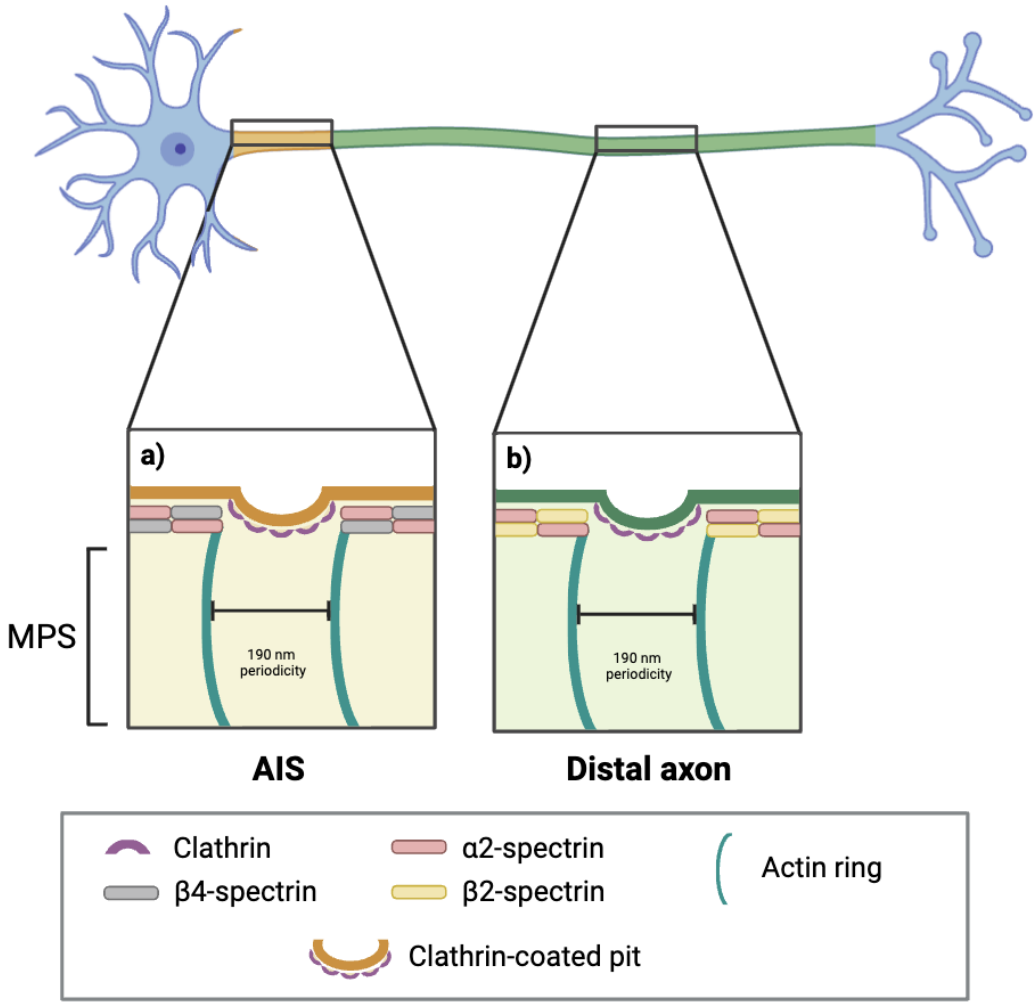

Figure 1: Schematic representation of the organization of the MPS at the AIS and distal axon.
A. Organization of the MPS at the AIS. At the AIS the MPS exists out of tetramers consisting of β4-spectrin, which is only expressed at the AIS, and α2-spectrin regulary interspaced every 190 nm with actin rings. Clathrin-coated pits can be found covering the surface of the plasma membrane in clearings of the MPS. **B.** Organization of the MPS at the distal axon. At the distal axon the MPS exists out of tetramers consisting of β2-spectrin and α2-spectrin regulary interspaced every 190 nm with actin rings. Also here, clathrin-coated pits can be found covering the surface of the plasma membrane in clearings of the MPS. Image made with Biorender.

neurons using N-methyl-D-aspartate (NMDA), which causes elevated neuronal activity and long-term depression (LTD) (11, 23). This indicates that CME along the axon becomes important in conditions of high neuronal activity which requires CCPs to be fully formed and "ready-to-go". However, how NMDA stimulates CME is not clear, but the mechanism seems to be complementary to the arrangement of the MPS.

During this research project, I observed the effect of diamide and NMDA on spectrin and actin periodicity and CCP formation. Together with the team, I also participated in the revision of the article of Wernert, Moparthi *et al.* in which we aim to shed light on how NMDA enables CME to occur along the axonal shaft of the AIS. We hypothesized that CME is stimulated by actin polymerization around the ~300 nm clearings along the AIS. To answer our research question, we use advanced microscopy techniques to resolve the 190 nm periodicity of the MPS and the CCP polymerized actin in both neurons with intact and pharmacologically perturbed MPS. A more profound understanding of how the axonal architecture uniquely regulates CME potentially offers new understandings in the pathophysiology and therapy development of several neurological diseases in future research.

EXPERIMENTAL PROCEDURES

Animals and neuronal cultures – For all the performed experiments, the use of Wistar rats was approved by the local ethics committee

(agreement D13-055-8). Pregnant dams and their embryos at 18 days of gestation were sacrificed in line with the guidelines of the European Animal Care and Use Committee (86/609/CEE). The cells were then brought into culture following the Banker method, suspended above a feeder glia layer to obtain a low-density culture (24). Isolated hippocampi were dissociated using a trypsin treatment following mechanical trituration. Neurons were subsequently seeded at a density of 4000-8000 cells/cm^2 on 18 mm round 1,5H coverslips coated with poly-L-lysine (Sigma-Aldrich #P2636), which has been shown to enhance the adhesion and maturation of neuronal cell cultures (25). After seeding, neurons were incubated for 3h in a serum-containing plating medium (Minimum Essential Medium 1X (MEM) Gibco #21090-022, D-glucose 20% Thermo Fisher #15023-021, sodium pyruvate Gibco #11360-039, Fetal Bovine Serum (FBS) Gibco #A3160801, Penicillin/Streptomycin Thermo Fisher #15140-122) to allow proper adherence to the coverslips. Thereafter, coverslips with adhered neurons were transferred to astrocyte cultures in Neurobasal+ (NB+) medium (Neurobasal® Medium (NB) 1X Gibco #21103049, B27 Thermo Fisher #17504-044, Penicillin/Streptomycin Thermo Fisher #15140-122, Amphotericin 100X Thermo Fisher #15290-026, L-glutamine 100X Thermo Fisher #25030-024). To suspend the coverslips above the astrocyte co-culture, paraffin dots were applied to the coverslips before seeding. Co-cultures were incubated at 37°C and 5% CO_2 for up to two weeks to allow the MPS to fully develop. Neurons were used for experimental purposes between 13-15 days *in vitro* (DIV).

Pharmacological treatments – For the diamide experiments, treatment of 14 DIV hippocampal neurons was done in their original conditioned NB+ medium for 45 minutes with 500 µM diamide. We found that using the original cell medium is the most optimal way to avoid cell stress. Dimethyl sulfoxide (DMSO, Sigma-Aldrich #D2650) was used at 0,1% as a control. After diamide treatment, cells were immediately fixed in an optimized paraformaldehyde (PFA)/PIPES, EGTA, and $MgSO_4$ (PEM) fixation solution (4% PFA, 4% sucrose, PEM) to avoid artifacts during SIM or STORM imaging (26). Fixation was performed at room temperature for 10 minutes. For treatment with N-Methyl-D-Aspartate (NMDA Sigma Aldrich #3262), 14 DIV neurons were pretreated for 5 minutes in unsupplemented NB medium. After pretreatment, 0.1 mM NMDA was added to the coverslips, and were subsequently incubated for 4 minutes in the incubator at 37°C and 5% CO_2. After treatment, coverslips were rinsed 3 times in fresh uncomplemented NB, transferred to their original conditioned NB+ medium, and put back in the incubator for 30 minutes at 37°C and 5% CO_2. Uncomplemented NB medium was used as a control. Immediately after treatment, neurons were fixed as previously described above.

Fluorescence immunocytochemistry – Standard fluorescence immunolabeling was performed by following published protocols (27). Samples were blocked and permeabilized for 1 h in immunocytochemistry (ICC) blocking buffer (0,2M phosphate buffer; Na_2HPO_4 Sigma-Aldrich #S0876 NaH_2PO_4 Sigma-Aldrich #S0751, 0,22% gelatin Sigma-Aldrich #G9391-500G) with 0,1% Triton X-100 at room temperature. When labeling for clathrin, blocking was performed for three hours instead of one hour. During blocking, samples were put on a rocking table for continuous agitation. Paraffin dots were removed from the coverslips within the last 5 minutes of blocking. Primary antibodies were subsequently incubated overnight at 4°C in ICC+0,1% Triton X-100 buffer, coverslips facing down. The following day coverslips were rinsed with ICC+0,1% Triton X-100 before secondary antibody incubation. Secondary antibody incubation was conducted for 1h at room temperature in ICC+0,1% Triton X-100, cells facing up. After secondary incubation, coverslips were rinsed twice with ICC+0,1% Triton X-100 and twice with phosphate buffer.

Primary and secondary antibodies – The following primary antibodies were used for immunolabeling of fixed hippocampal neurons; chicken polyclonal anti-MAP2 (1:1000) (Synaptic Systems #188006), guinea pig polyclonal anti-clathrin light chain (CLC) (1:500) (Synaptic Systems #113004), mouse monoclonal anti-β2-spectrin (1:100) (BD Biosciences #612563), mouse monoclonal anti-α2-spectrin (1:100) (BioLegend #803201), rabbit polyclonal anti-β4-spectrin (1:500) (Matthew Rasband, Baylor College of

Medicine, Austin, Texas). For secondary antibody incubation the following secondary antibodies were added to the coverslips; goat anti-chicken conjugated to DyeLight (DL) 405 (1:200) (Tebubio #603146126), goat anti-guinea pig conjugated to Alexa Fluor (AF) 488 (1:400) (Invitrogen #A11073), donkey anti-mouse conjugated to AF555 (1:400) (Invitrogen #A31570), donkey anti-rabbit conjugated to AF647 (1:300) (Invitrogen #A31573). For post-actin staining, Phalloidin Atto488 (Atto-Tec #AD48881) was used in case of SIM imaging and Phalloidin AF647+ (Thermo Fisher #A30107) when destined for STORM imaging.

Unroofing – To prepare neurons for unroofing, they were immersed in three subsequent preheated solutions; First, they were quickly rinsed three times in a calcium-enriched Ringer solution (155 mM NaCl, 3 mM KCl, 3 mM NaH_2PO_4, 5 mM HEPES, 10 mM glucose, 2 mM $CaCl_2$, 1 mM $MgCl_2$, pH 7.2) to rinse away NB+ medium. They were next placed in Ringer solution containing 0.5 mg/ml poly-L-lysine (155 mM NaCl, 3 mM KCl, 3 mM NaH_2PO_4, 5 mM HEPES, 10 mM glucose, 3 mM EGTA, 5 mM $MgCl_2$, pH 7.2) for 10 s. Lastly, they were quickly immersed in Ringer solution without enriched calcium to detach excess poly-L-lysine. Afterward, neurons were unroofed in KHMgE buffer (70 mM KCl, 30 mM HEPES, 5 mM MgCl2, 3 mM EGTA, pH 7.2) by sonicating with 2-5 s sonicator pulses at ~2.5 mm distance of the cells using a probe sonicator (4 mm tip, 20% amplitude, angle at ≥ 45°, Sonics Vibra Cell™) at the lowest deliverable power. Unroofed neurons were immediately fixed after sonication for 15 min in KHMgE with 4% PFA. Before immunolabeling samples were rinsed 3 times with KHMgE. Immunolabeling was performed in the same way as described above, but instead of ICC buffer with 0,1% Triton X-100, a detergent-free buffer (KHMgE, 1% BSA) was used.

Dextran and MemGlow uptake assays – For the dextran uptake assay, hippocampal neurons were treated for 4 minutes with a final concentration of 50 µM NMDA (from 50 mM stock diluted in ultrapure water, Sigma-Aldrich #M3262) at 37°C and 5% CO_2. Unsupplemented NB medium was used as a control. After 4 minutes, neurons were rinsed 3 times, transferred into their original dishes with conditioned NB+, and placed back into the incubator for 30 minutes of rest. Subsequently, neurons were incubated at 37°C and 5% CO_2 with dextran 10 kDa conjugated to Alexa Fluor 555 (Thermo Fisher Scientific #D34679) for 30 minutes. Immediately after the uptake assay, neurons were fixed for 10 minutes in 4% PFA, 4% sucrose, and PEM buffer. Throughout the whole experiment, unsupplemented NB medium and reagents were kept at 37°C. During the entirety of the experiment, neurons were exposed to 5 µM latrunculin A (Sigma-Aldrich #L5163) or 100 µM calpain inhibitor (MDL 28170 Merck #M6690), except for the NMDA and control condition. Immediately after the uptake assay, neurons were rinsed three times by dipping them in unsupplemented NB and fixed for 10 minutes in 4% PFA, 4% sucrose, and PEM buffer. For the duration of the experiment, NB medium and dextran-AF555 were kept at 37°C.

For the MemGlow uptake assay, the same experimental procedure was followed as for the dextran uptake assay. MemGlow560 was used at 200 nM. Fixation was carried out for 20 minutes instead of 10 minutes, due to the lipid properties of Memglow560. In order to avoid washing away the cell membrane during immunostaining, a detergent-free buffer (ICC buffer without Triton X-100) was used after an hour of membrane permeabilization and blocking step.

Structured illumination microscopy – Fixed hippocampal neurons were imaged on an N-SIM-S inverted Nikon Eclipse Ti2-E microscope (Nikon Instruments) on their respective 18 mm coverslips mounted in ProLong™ Glass Antifade Mountant (Thermo Fisher Scientific #P36980). The N-SIM-S microscope is equipped with four laser channels at excitation wavelengths of 405, 488, 561 and, 640 nm, a Mad City Labs Nanodrive piezo stage and, a Hamamatsu Fusion BT CMOS camera. The AIS of neurons of interest were located with a 100X NA 1.49 oil objective and images were acquired in 3D-SIM mode (17 planes per image). After acquiring the z planes of the images, they were reconstructed by the NIS-elements software.

SMLM: STORM – 2D STORM imaging of the AIS of hippocampal neurons was performed on a widefield N-STORM microscope (Nikon Instruments). Prior to

imaging, a STORM buffer was prepared, consisting of a saline buffer (Smart Buffer Kit Abbelight), an enzymatic oxygen scavenger system consisting of catalase and glucose oxidase (GLOX) (Smart Buffer Kit Abbelight) to minimalize photobleaching due to oxygen radical formation, and mercaptoethylamine (MEA) (cysteamine, Merck #30070-10G, 1M stock in 360 mM HCl), which allows blinking of fluorophores. Stained coverslips were subsequently mounted in a silicon chamber filled with STORM buffer. The AIS of neurons of interest were located with a 100X NA 1.49 oil objective. After localizing a region of interest (ROI), a super-resolved image was taken at 647 nm at the TIRF critical angle (Highly Inclined and Laminated Optical sheet HILO modality). Stained hippocampal neurons were kept in sodium azide (Sigma-Aldrich #S20025G) and phosphate buffer to store the samples for up several weeks. In case actin was imaged, coverslips were kept in phalloidin Atto 647+ (1:400) and were stored at 4°C in a humidified chamber for up to 4 days.

Live cell imaging – Neurons were mounted in a metal chamber on their coverslip and rinsed three times with Hibernate+ (2% B27 Thermo Fisher #17504-044, 0,5 mM L-glutamine Thermo Fisher #25030-024, 2,5 M 20% glucose Thermo Fisher #15023-021, 1X Hibernate® E medium low fluorescence TransnetYX #022024). Hibernate+ was also used as the imaging medium. For actin staining, GR555 (100 µM stock solution in anhydrous DMSO, gifted by Zhixing Chen, Beijing) or SPY555 (100 µM stock solution in anhydrous DMSO, Spirochrome #SC202) were used, while for staining of the plasma membrane PKMem560 (100 µM stock solution in anhydrous DMSO, gifted by Zhixing Chen, Beijing) or MemGlow560 (100 µM stock solution, Cytoskeleton #MG02-02) were used to label neurons. The probes were added to the imaging medium to a final concentration of 100 nM. Subsequently, live cell imaging was performed on a N-SIM-S inverted Nikon Eclipse Ti2-E microscope (Nikon Instruments) in case actin periodicity needed to be observed, or on an inverted Nikon Eclipse Ti2-E microscope equipped with an Omicron LightHub 4-line laser unit, a CSU-W1 SoRa module (Yokogawa CSU series), an MCL Z drive and a PFS. During live cell imaging neurons were kept in a humidified cage incubator at 37°C.

Data quantification and analysis – MPS periodicity was quantified by determining the autocorrelation intensity profile in Fiji (version 2.14.0/1.54i) from line ROIs along the AIS, calculated with a Fiji script (https://github.com/cleterrier/Process_Profiles/blob/master/Autocorrelation_.js). To determine the average autocorrelation at 190 nm the following formula was used:

$$\boldsymbol{Amplitude_{max}} - \left(\frac{(\boldsymbol{Amplitude_{min,left}} + \boldsymbol{Amplitude_{min,right}})}{\mathbf{2}}\right)$$

Clathrin pit and dextran density were analyzed on a plugin on Fiji (version 2.14.0/1.54i). StarDist was used to segment densely packed objects from threshold images (28). Thresholding was done with Moments for clathrin pits, while for thresholding dextran Otsu was used.

Bleaching on time-lapses of neurons acquired by live cell imaging was quantified using a custom Fiji macro (https://github.com/julliennicolas/LiveCellBleach.git). To quantify the photobleaching of the PK Mem and Memglow560 staining, the mean intensity over the image with subtracted background was measured for each frame.

Statistics – Statistical analysis was performed on GraphPad Prism software (version 9.5.0). Significances were tested using Mann-Whitney U test to compare unpaired non-parametric data or a Kruskal-Wallis test for multiple comparisons. Data were found to be significant at a significance level $\alpha \leq 0.05$. In figures, obtained p values are indicated as follows: ns, non-significant; *, $p < 0.05$; **, $p < 0.01$; ***, $p < 0.001$; ****, $p < 0.0001$. Experiments were carried out in duplicate for reproducibility.

RESULTS

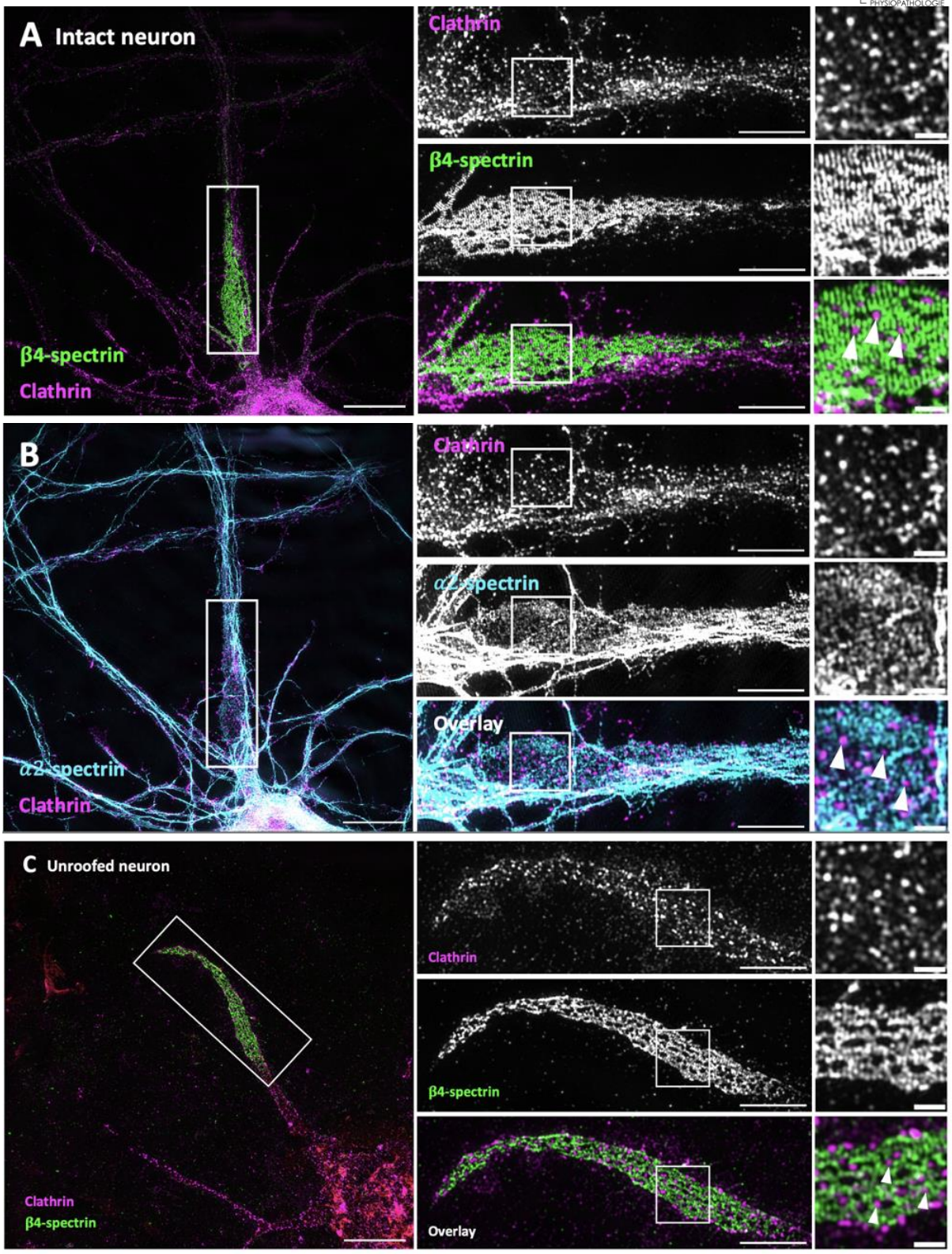

Clathrin pits form in clearings of the spectrin scaffold along the AIS – To investigate whether CCPs reside in clearings of the MPS, SIM was used to image the AIS of hippocampal neurons. SIM uses rotating diffraction gratings to produce a structured light pattern of Moiré fringes with modulations below the diffraction limit (29). The patterned interferences enhance spatial resolution in the image with a lateral resolution of ~120 nm resolution and an axial resolution of ~250 nm for 3D-SIM (8, 29). This is sufficient to visualize 190 nm periodicity of the MPS and individual CCPs (8, 11). In addition, SIM also offers a large field of view

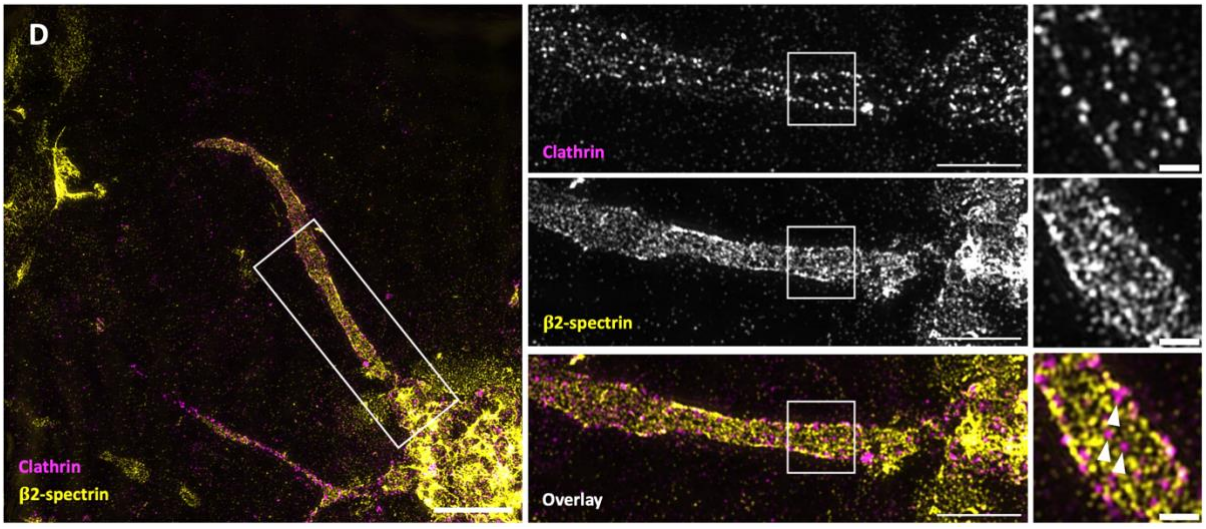

Figure 2: Clathrin pits form in clearings of the spectrin scaffold at the AIS.
A. SIM image of a cultured hippocampal neuron at 14 DIV fixed and stained for clathrin light chain (CLC) (magenta, CCPs appear as clusters) and β4-spectrin (green, AIS-specific with visible 190 nm recurring periodicity). Central images show zooms of the AIS corresponding to the indicated area on the left image, square images in the center column show zooms of areas of interest on the AIS. CCPs residing in clearings are indicated with white arrowheads. Scale bars; 10 µm (left image), 5 µm (center column), 1 µm (right square zoomed images). **B.** Same SIM image as in panel A, but showing an overlay of stained clathrin (magenta, CCPs appear as clusters) and α2-spectrin. Central images show zooms of the AIS corresponding to the indicated area on the left image, square images in the center column show zooms of areas of interest on the AIS. CCPs residing in clearings are indicated with white arrowheads. Scale bars; 10 µm (left image), 5 µm (center column), 1 µm (right square zoomed images). **C.** SIM image of a 30 DIV unroofed, fixed and stained neuron. The neuron was stained for clathrin (magenta, CCPs appear as clusters) and β4-spectrin (green, AIS-specific). Central images show zooms of the AIS corresponding to the indicated area on the left image, square images in the center column show zooms of areas of interest on the AIS. CCPs residing in clearings are indicated with white arrowheads. Scale bars, 10 µm (left image), 5 µm (center column), 1 µm (square zoomed images). **D.** Same SIM image as in panel C, but showing an overlay of stained clathrin (magenta, CCPs appear as clusters) and β2-spectrin. Central images show zooms of the distal axon corresponding to the indicated area on the left image, square images in the center column show zooms of areas of interest on the distal axon. CCPs residing in clearings are indicated with white arrowheads. Scale bars; 10 µm (left image), 5 µm (center column), 1 µm (right square zoomed images).

(FOV) and is relatively easier to use and faster than SMLM (8, 11). As confirmed by the paper of Wernert, Moparthi *et al.*, ~100 nm CCPs are found in areas devoid of spectrin mesh (11). CCP clearings at the AIS are both devoid of β4-spectrin and α2-spectrin (**figure 2A-B**, white arrowheads). To obtain more defined images of the clearings, mechanical unroofing of neurons was performed. This technique uses sonication to remove the upper surface of the plasma membrane and reveals structures of the ventral membrane, which corresponds to the inner side of the plasma membrane (30). By applying unroofing, it is therefore, possible to get more defined and prominent views on CCPs residing in clearings at the ventral side of the membrane (**figure 2C**, white arrowheads). During the unroofing process, intracellular protein components are removed as well, which also improves the visualization of clearings in the spectrin mesh (30).
With the help of unroofing, CCPs were also observed to be present in clearings devoid of β2-spectrin at the level of the distal axon (**figure 2D**, white arrowheads). PREM data in Wernert, Moparthi *et al.* indicate that the diameter of the clearings in which the CCPs are found is ~300 nm (11). It was not possible to measure the diameter of individual clearings with the SIM data generated for this report, because of the limited resolution of SIM compared to PREM, but we confirmed that CCPs are found inside clearings of the spectrin mesh.

Pharmacological perturbation of the MPS causes increased CCP formation – Based on the comprehension that CCPs only form in clearings of the spectrin mesh, it can be tested whether CCP formation can be stimulated by pharmacological perturbation of the mesh. To reveal whether perturbing the spectrin mesh would elevate CCP density, neurons were treated with diamide, which is a drug that oxidizes spectrins and disrupts its organization within the MPS (11, 31, 32). Before comparing CCP density in control versus diamide-treated neurons, the perturbing effect of diamide on β4-spectrin was validated. The AIS of hippocampal neurons treated with diamide

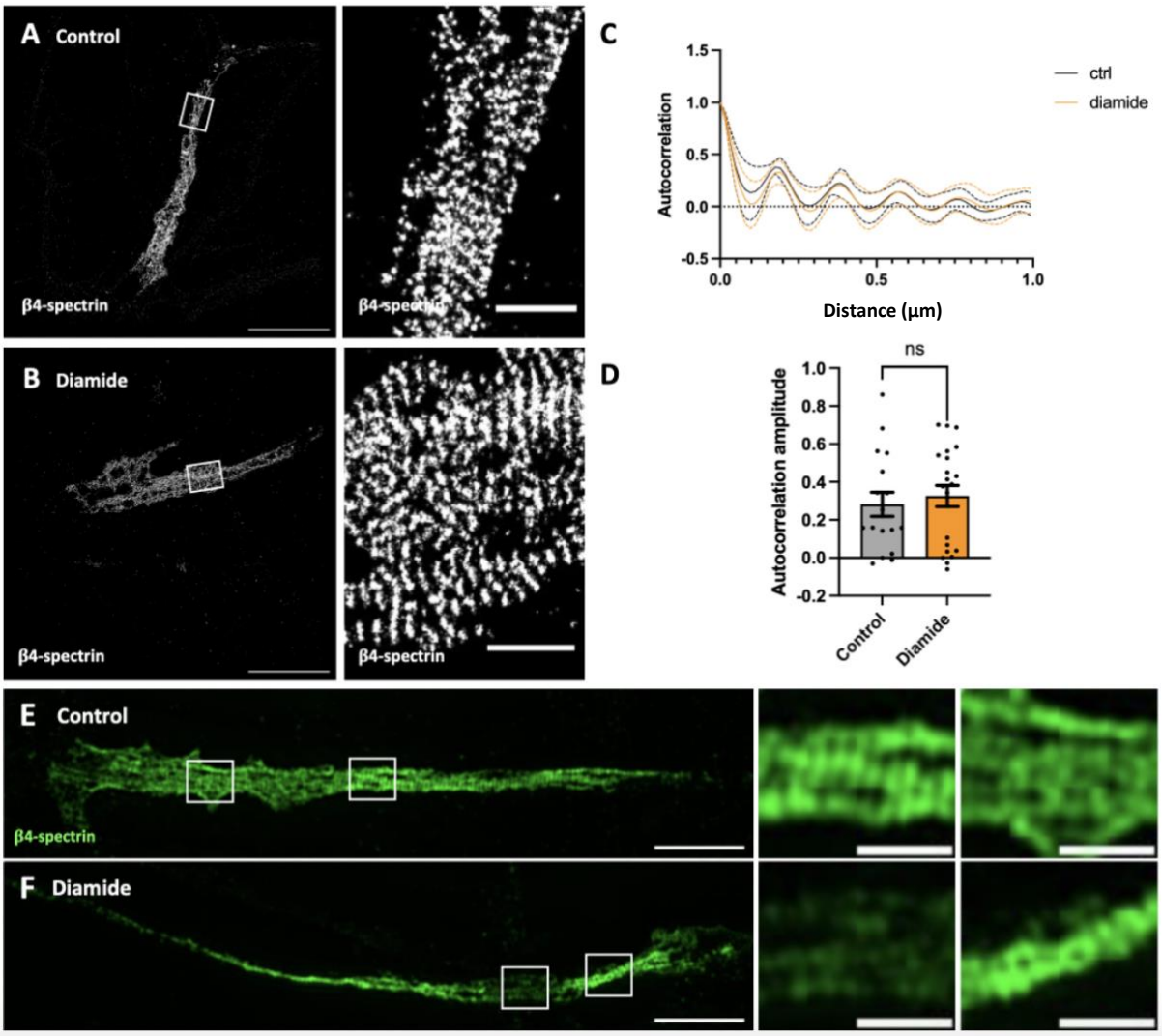

Figure 3: Pharmacological treatment with diamide partially influences β4-spectrin periodicity.
A-B. STORM images of AIS of cultured hippocampal neurons at 14 DIV treated with control (0.1% DMSO for 45 minutes) or diamide (5 mM for 45 minutes). Neurons were fixed and stained for β4-spectrin (AIS-specific, visible 190 nm periodicity). Images at the right show zooms of the AIS corresponding to the indicated area on the left images. Scale bars; 10 µm (left images), 1 µm (right images). **C.** Graph showing the autocorrelation profiles of control versus diamide-treated hippocampal neurons along the AIS. **D.** Bar plots showing the average amplitudes of the autocorrelations of control (N = 17) versus diamide (N = 22) treated neurons at 190 nm. A comparison of ranks with a Mann-Whitney U test was used to obtain p values. Significance level $\alpha > 0.05$ ($p = 0.5609$). **E-F.** SIM images of 14 DIV hippocampal neurons treated as in figure A and B. Neurons were fixed and stained for β4-spectrin (green, AIS-specific). Scale bars; 4 µm (left images), 1 µm (right images, zooms of the corresponding white boxes in the left images).

were imaged using 2D-STORM. STORM is an imaging technique that resolves structural information beyond the diffraction limit by means of single molecule localization microscopy (SMLM). In diffraction limited imaging, a high density of single fluorescent emitters crowd the image with overlapping point spread functions (PSF) which cannot be individually resolved. In SMLM, random subsets of these fluorophores are cycled through bright and dark states so that no two PSF overlap in the resulting image. These non-overlapping PSF can be fitted with a Gaussian function, which is going to approximate the center of the fluorophore, reaching a lateral resolution of up to ~20 nm. With a ~20 nm lateral resolution, STORM can resolve MPS periodicity with a higher resolution than SIM (8). The obtained lateral resolution of STORM thus allows quantification of the MPS periodicity, which is not possible with SIM data. Obtained STORM images reveal that the 190 nm periodicity of β4-spectrin was preserved in diamide-treated neurons compared to the control (**figure 3A-B**). This observation was confirmed by the autocorrelation and the average amplitude at 190 nm (**figure 3C-D**). The autocorrelation profile of diamide-treated neurons was found similar to that of the control condition (**figure 3C**). Comparison of the

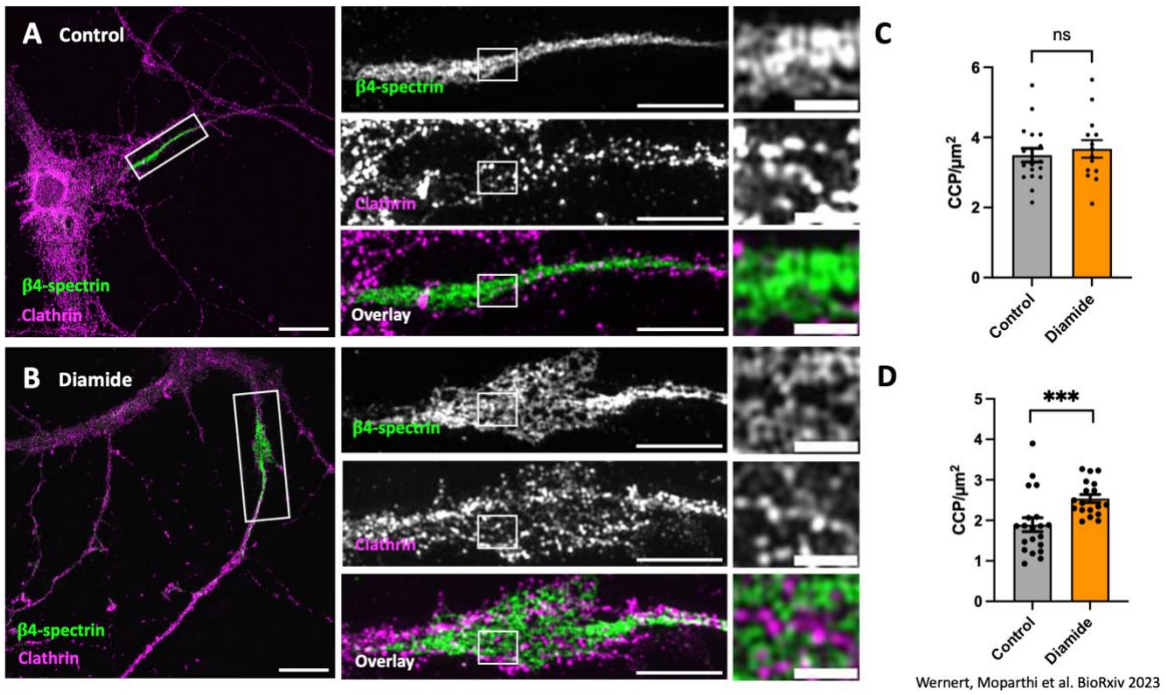

Figure 4: Pharmacological treatment with diamide increases clathrin pit formation along the AIS.

A-B. SIM images of 14 DIV cultured hippocampal neurons treated with control (0.1% DMSO for 45 minutes) or diamide (5 mM for 45 minutes). Neurons were fixed and stained for clathrin-light-chain (CLC) (magenta) and β4-spectrin (green). Scale bars; 10 µm (left images), 4 µm (center columns), 1 µm (right images, zooms of the corresponding white boxes in the middle columns). **C.** Bar plots showing the CCP density per µm^2 of the AIS of neurons treated with control (N = 18) or diamide (N = 14). Comparison of ranks with a Mann-Whitney U test was performed to obtain p values. Significance level $\alpha > 0.05$ (p = 0.6666). Data obtained from own experiments during internship. **D.** Bar plots showing the CCP density per µm^2 of the AIS of neurons treated with control (N = 20) or diamide (N = 18). Comparison of ranks with a Mann-Whitney U test was performed to obtain p values. Significance level $\alpha < 0.05$ (p = 0.0004). Quantification shown is from Wernert, Moparthi *et al,* 2023.

average amplitude at 190 nm of the two conditions was also found to be non-significant (mean ± SEM; 0.28 ± 0.06 for control, 0.32 ± 0.05 for diamide condition) (**figure 3D**). Conflicting results were found on SIM images, which showed diamide-treated neurons with regions of perturbed and dimmer β4-spectrin staining (**figure 3E-F**). It is suspected that diamide therefore partially disrupts the β4-spectrin mesh.

The same experiment was done for actin, but periodicity was difficult to visualize due to formation of long actin filaments and a high degree of fasciculation of neurites likely induced during the treatment process (**supplementary figure 1,2**). Therefore, STORM images of actin were unusable for reliable quantification of the actin periodicity.

SIM images were obtained to look at the effect of diamide on CCP formation at the AIS (**figure 4A-B**). Quantifying these experiments did not give results consistent with the data in Wernert, Moparthi *et al.* (mean ± SEM; 3.49 ± 0.19 for control, 3.67 ± 0.25 for diamide condition) (**figure 4C**) (11). Previously conducted experiments showed that diamide led to a significant increase in CCP density at the AIS (mean ± SEM; 1.89 ± 0.17 for control, 2.54 ± 0.10 for diamide condition, p-value = 0.0004) (**figure 4D**) (11). Pharmacological perturbation of the spectrin mesh thus results in an increase of CCPs at the AIS.

NMDA-induced elevated neuronal activity partially impacts the spectrin scaffold at the AIS – To investigate whether elevated neuronal activity affects β4-spectrin periodicity at the AIS, NMDA was used to induce long-term depression (LTD) (33). STORM images of neurons treated with NMDA show visible disorganization (**figure 5A-B**). This observation is supported by the autocorrelation profile of NMDA-treated neurons, of which

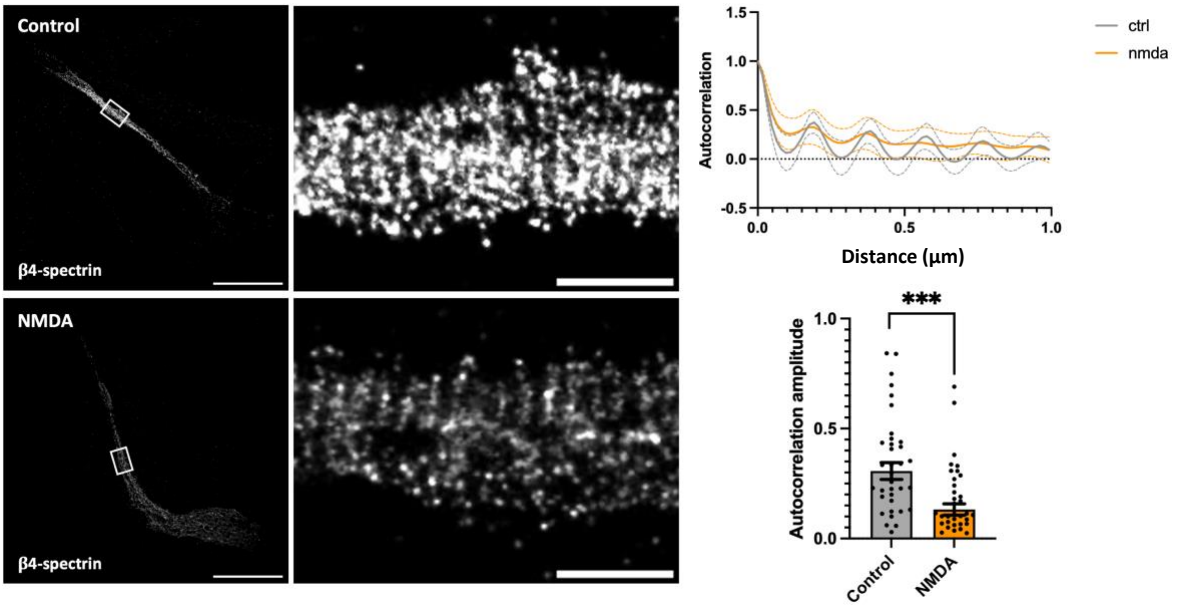

Figure 5: Elevated neuronal activity induced with NMDA disorganizes β4-spectrin periodicity at the AIS.

A-B. STORM images of AIS of cultured hippocampal neurons at 15 DIV treated with control (uncomplemented NB) or NMDA (50 µM for 4 minutes + 30 minutes rest). Neurons were fixed and stained for β4-spectrin (AIS-specific, visible 190 nm periodicity in control image, completely perturbed in NMDA image). Images at the right show zooms of the AIS corresponding to the indicated areas on the left images. Scale bars; 10 µm (left images), 1 µm (right images). **C.** Graph showing the autocorrelation profiles of β4-spectrin periodicity at the AIS in control versus NMDA-treated hippocampal neurons. **D.** Bar plots showing the average amplitudes of the autocorrelations of control (N = 38) versus NMDA (N = 43) treated neurons at 190 nm. A Mann-Whitney U test was performed to compare ranks and obtain p values. Significance level $\alpha < 0.05$ ($p = 0.0001$).

autocorrelation is attenuated compared to the autocorrelation profile of the control condition (**figure 5C**). Comparison of the average amplitudes at 190 nm of the NMDA-treated condition and control condition shows a significant decrease in β4-spectrin periodicity in NMDA-treated neurons (mean ± SEM; 0.30 ± 0.03 for control, 0.13 ± 0.02 for NMDA condition, p-value = 0.0001) (**figure 5D**).

The same experiment was done for actin, but as previously mentioned, STORM data could not be quantified due to similar reasons (**supplementary figure 1,3**). Therefore, generated STORM images of actin were again unusable for reliable quantification of the actin periodicity.

Based on the obtained STORM data, it can be confirmed that β4-spectrin periodicity is still detectable after NMDA-induced LTD but is significantly attenuated.

Elevated neuronal activity increases clathrin-mediated endocytosis – After confirming the effect of NMDA on β4-spectrin organization, it was explored whether NMDA also affects CCP formation and clathrin-mediated endocytic (CME) events. CME was visualized by performing uptake assays using fluorescently labeled dextran (10 kDa).

After performing the uptake assay with dextran-555, SIM data revealed a significant increase in dextran uptake at the AIS of NMDA-treated neurons compared to the control (mean ± SEM; 1.63 ± 0.08 for control, 2.21 ± 0.12 for NMDA condition; p (control vs NMDA) = 0.0145) (**figure 6B-C,H**, quantifications performed by F. Wernert). This data was supported by staining the neuronal plasma membrane with Memglow560, a membrane lipid conjugated to Cy3, to visualize cargo internalization in endosomal compartments as an extra validation for CME to occur at the AIS (**supplementary figure 5**). However, no significant increase in CCP formation at the AIS was observed compared to the control (mean ± SEM; 2.35 ± 0.21 for control, 3.06 ± 0.19 for NMDA condition) (**figure 6B-C,I)**. Therefore, it can be assumed that NMDA has a regulating effect on CME, but does not affect CCP formation.

Elevated neuronal activity stimulates actin polymerization around clathrin pits – The preprint version of Wernert et al. suggested that in addition to the formation of CCPs within clearings of the spectrin mesh, actin

polymerization around the CCPs is necessary for CME to occur, due to the appearance of dense actin within clearings on PREM images (**figure 6A**). To investigate the possible underlying mechanism of increased endocytosis and the factors that might play a role in this, neurons were additionally treated with latrunculin A and calpain inhibitor after NMDA treatment (**Supplementary figure 4**). Latrunculin A is a drug that interferes with polymerized actin by binding to actin monomers or depolymerizing already existing actin filaments (34). This drug therefore reveals the involvement of actin polymerization in the heightened occurrence of endocytosis along the AIS. Additionally, a calpain inhibitor (CI) was added to the experiment because calpain, a calcium-dependent cysteine protease, has been known to be a potent mediator of spectrin proteolysis by cleaving its binding sites at the plasma membrane (35). Calpain could therefore play a role in the observed increase of endocytic events at the AIS (36, 37). The obtained SIM data shows a comparison between AIS stained for clathrin and dextran-555 (**figure 6B-E**). A significant decrease in dextran-555 uptake was observed in the CI-treated condition compared to the control and NMDA condition, while there was only a significant decrease of dextran uptake in the latrunculin A condition compared to the NMDA condition (mean ± SEM; 1.63 ± 0.08 for control, 2.21 ± 0.12 for NMDA condition, 1.53 ± 0.08 for latrunculin A+NMDA condition, 0.56 ± 0.051 for CI+NMDA condition; p (control vs NMDA) = 0.0145; p (control vs CI) = 0.0001; p (NMDA vs LatA) = 0.0026; p (NMDA vs CI) = < 0.0001; p (LatA vs CI) = 0.0016) (**figure 6H**). In the case of CCP formation, there was a significant decrease on CCP formation in the CI condition compared to control and NMDA condition. CCP formation in the latrunculin A condition was also found to be decreased significantly compared to the NMDA condition (mean ± SEM; 2.35 ± 0.21 for control, 3.06 ± 0.19 for NMDA condition, 1.44 ± 0.14 for latrunculin A+NMDA condition, 0.68 ± 0.08 for CI+NMDA condition; p (control vs CI) = < 0.0001; p (NMDA vs LatA) = 0.0002; p (NMDA vs CI) = < 0.0001) (**figure 6I**). Consistent with the significant decrease in dextran-555 uptake and CCP formation in the latrunculin A condition compared to the NMDA condition, polymerized actin was observed around CCPs in SIM images of unroofed neurons treated with NMDA and was found to be absent in latrunculin A SIM images (**figure 6F**, arrowheads). SIM images of unroofed neurons treated with CI are lacking and are therefore not shown.

Based on the SIM results, it can be concluded that NMDA-induced LTD is necessary for actin to polymerize around CCPs and unlock CME. However, CCP formation is independent of elevated neuronal activation.

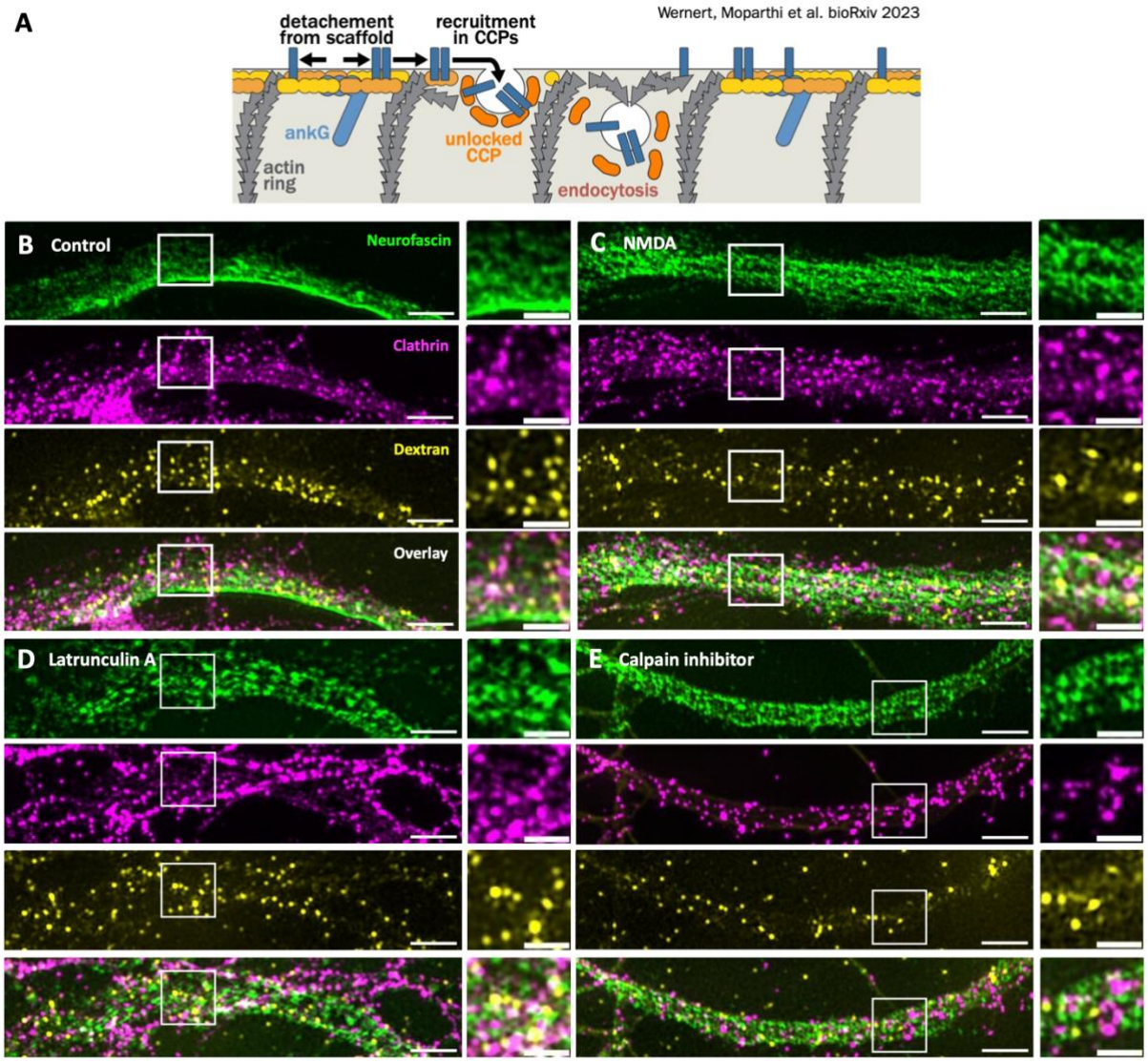
A
detachement from scaffold
recruitment in CCPs
Wernert, Moparthi et al. bioRxiv 2023
ankG
actin ring
unlocked CCP
endocytosis
B Control
Neurofascin
Clathrin
Dextran
Overlay
C NMDA
D Latrunculin A
E Calpain inhibitor

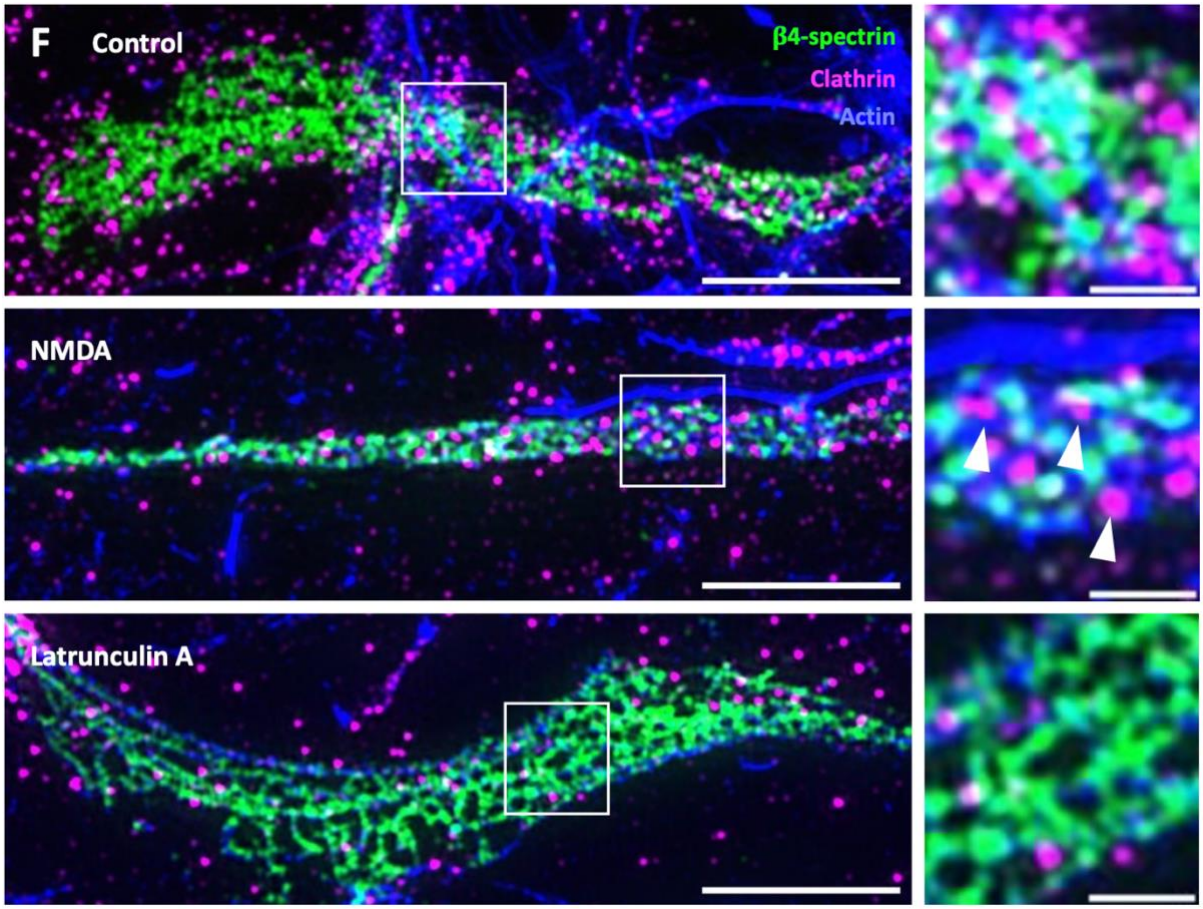
F
Control
β4-spectrin
Clathrin
Actin
NMDA
Latrunculin A

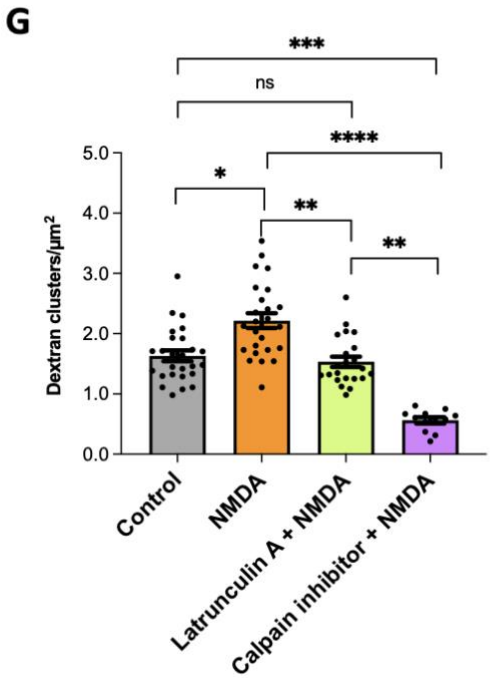
G
Dextran clusters/µm²
5.0
4.0
3.0
2.0
1.0
0.0
***
ns
****
*
**
**
Control
NMDA
Latrunculin A + NMDA
Calpain inhibitor + NMDA

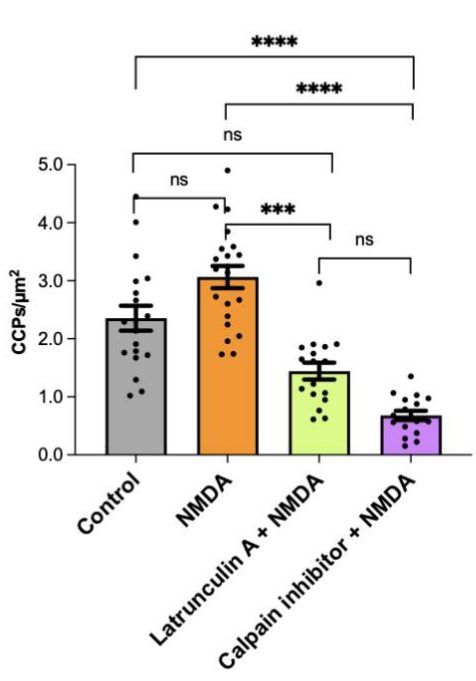
H
CCPs/µm²
5.0
4.0
3.0
2.0
1.0
0.0
****
****
ns
ns
***
ns
Control
NMDA
Latrunculin A + NMDA
Calpain inhibitor + NMDA

Figure 6: Elevated neuronal activity induced by NMDA increases clathrin-mediated endocytosis and stimulates the polymerization of actin around clathrin pits.

A. Schematic representation showing the proposed two-step mechanism necessary for clathrin-mediated endocytosis to occur at the AIS. Firstly, the area must be cleared of spectrin scaffold to allow CCPs to form on the bare plasma membrane. Secondly, actin needs to polymerize at the surface to aid in the scission of the CCP. Figure originating from Wernert, Moparthi *et al.* 2023. **B-E.** SIM images of AIS of cultured hippocampal neurons at 14 DIV treated with control (uncomplemented NB), NMDA (50 µM for 4 minutes), NMDA (50 µM for 4 min) + latrunculin A (LatA) (5 µM during 4 min of NMDA treatment, 30 min of rest and 30 minutes of feeding), NMDA + calpain inhibitor (CI) (100 µM during 4 min of NMDA treatment, 30 min of rest and 30 minutes of feeding). Neurons were fixed and stained for neurofascin (labels AIS) (green) and CLC (magenta). Fluorescently labeled 10 kDa AF555-dextran (yellow) was added to neurons to visualize endocytosis along the AIS. Images at the right show zooms of regions of interest of the AIS corresponding to the indicated areas on the left image. Scale bars; 2 µm (left images), 1 µm (right images). **F.** SIM images of 14 DIV unroofed neurons fixed and stained for β4-spectrin (AIS-specific), CLC (magenta), and actin (blue). Images at the right show zooms of regions of interest corresponding to the white boxes in the left images. Arrowheads show CCPs surrounded with polymerized actin. Scale bars; 5 µm (left images), 1 µm (right images). **G.** Bar plots showing the density of dextran clusters/µm^2 of AIS treated with control (N = 26), NMDA (N = 25), NMDA+latrunculin A (N = 22), and NMDA+calpain inhibitor (N = 12). A Kruskal-Wallis test was performed to compare the density of dextran clusters/µm^2 for every condition. p (control vs NMDA) = 0.0145; p (control vs LatA) = >0.9999; p (control vs CI) = 0.0001; p (NMDA vs LatA) = 0.0026; p (NMDA vs CI) = < 0.0001; p (LatA vs CI) = 0.0016. **H.** Bar plots showing the CCP density/µm^2 of AIS treated with control (N = 19), NMDA (N = 21), NMDA+latrunculin A (N = 17), and NMDA+calpain inhibitor (N = 17). A Kruskal-Wallis test was performed to compare the density of CCPs/µm^2 for every condition. p (control vs NMDA) = 0.5485; p (control vs LatA)= 0.0870; p (control vs CI) = < 0.0001; p (NMDA vs LatA) = 0.0002; p (NMDA vs CI) = < 0.0001; p (LatA vs CI) = 0,1072.

DISCUSSION

Clathrin pits form in clearings of the spectrin scaffold along the AIS – Endocytosis along the AIS and proximal axon has long been overlooked. Yet, the presence of CCPs along the AIS indicates that it has essential functions at the axon, such as the maintenance of axonal polarity and recycling of membrane receptors at the axonal plasma membrane (22, 38). Additionally, it could potentially also play a role in regulating the AIS length and neuronal excitability.

Our team previously showed that the MPS regulates CCP formation by organizing CCPs in clearings depleted of spectrin mesh (11). These structures have been observed earlier in diffraction-limited fluorescent microscopy images of mouse embryonic fibroblasts (MEFs) and epithelial cells (38, 39). The inability of clathrin pits to assemble at sites where MPS is present is linked to sterical hindrance of the spectrin scaffold as shown by Wernert, Moparthi. *et al.* β-spectrins directly interact with the cell membrane by binding to phosphatidylinositol lipids, occupying important binding sites for endocytic proteins such as clathrin adaptor protein 2 (AP2) and several cargo adaptors (40, 41). CCPs are therefore only able to form at the bare plasma membrane. By increasing the accessible plasma membrane surface more CCPs can be formed. These pits have been shown to be stalled in Wernert, Moparthi *et al.* It is proposed that this negative regulation avoids spontaneous endocytosis of important membrane proteins such as sodium channels that generate the action potential.

Pharmacological perturbation of the MPS causes increased CCP formation – Diamide has been proven to increase CCP density at the AIS by disrupting the spectrin mesh (11). Therefore, it was surprising to see that there was no significant effect of diamide on β4-spectrin periodicity (**figure 3D**). Wernert, Moparthi *et al.* show a visible, however partial effect of diamide on spectrin organization in the PREM images with the mesh transformed into connected globules, and therefore the generated results are not consistent with the article. There can be several explanations for the inconsistency. Firstly, it is possible that the diamide was ineffective. The first experiments were performed with 15 minutes of diamide compared to other experiments that were performed with 45 minutes of diamide treatment. It could be that the 15-minute treatment was insufficient for perturbation to happen. The used diamide could potentially also have been degraded and as a result did not manage to perturb spectrin. Secondly, it could be possible that the spectrin disorganization is not visible on STORM images and is only observable with PREM resolution. Lastly, it could be linked to experimental issues. Based on the observation that diamide increases CCP density but not endocytosis, it can be speculated that the MPS creates membrane tension which is not sufficiently decreased by the partial effect of diamide on the spectrin scaffold (42, 43). This reasoning can be supported by research showing that β-spectrins induce membrane tension along the axon and can therefore have an inhibitory effect on endocytosis (44). β-spectrins can therefore have an inhibitory effect on endocytic events.

NMDA-induced elevated neuronal activity impacts the spectrin scaffold at the AIS – The effect of NMDA on β4-spectrin periodicity is more consistent with the findings in Wernert, Moparthi *et al.* (11). Although, for the determined average autocorrelation, peaks at 190 nm are more prominent in the article of Wernert, Moparthi *et al.* The periodicity of β4-spectrin is therefore only partially affected by NMDA. The partial effect of NMDA on β4-spectrin periodicity could be explained by β4-spectrin being a very robust cytoskeletal component (3). As β4-spectrin is one of the main components of the MPS in the AIS, it is proven to be highly resistant to cytoskeletal perturbations because the AIS is crucial for action potential generation and therefore needs to withstand a lot of mechanical stress (3). In order to maintain its structural integrity, the AIS therefore needs to be studded with highly stable cytoskeletal assemblies. Also, for the axon to maintain its molecular identity, the AIS needs to stay intact (4).

Elevated neuronal activity increases clathrin-mediated endocytosis – NMDA-induced LTD has been shown to have an increasing effect on endocytosis but not on CCP formation (**figure 6G-H**). This suggests that NMDA predominantly acts upon stimulating CME to occur and does not necessarily act upon creating more holes within the spectrin scaffold

for CCP assembly. The increased endocytosis elicited with NMDA was additionally demonstrated with MemGlow, a membrane lipid that only fluoresces when incorporated into the plasma membrane (**supplementary figure 4**) (45). By using MemGlow, we could confirm endocytic events by looking at the endosomal components at the plasma membrane. A difference in the shape of endosomal compartments was visible along the plasma membrane. In the control condition, endosomal compartments in the AIS are present as tubulovesicular endosomes, while in the NMDA-treated neurons, small circular endosomal compartments can be observed. These small endosomal compartments along the AIS are likely indicating CME occurring (46). Furthermore, Memglow was compared to PK Mem, a fluorophore with self-healing properties, for future use in live cell imaging (**supplementary figure 5**). In literature, PK Mem is shown to reduce phototoxicity and enhance photostability, confirmed by our own live cell imaging experiments (**supplementary figure 5**).

Elevated neuronal activity stimulates actin polymerization around clathrin pits – The underlying mechanism behind the increased CME is likely stimulated by actin polymerization around CCPs that pull the pits inward. The promoting effect that branched actin has on severing and invaginating CCPs was already observed in previous research in which this mechanism is presented as the "edge pushing" model for CME (47). The effect of NMDA on actin polymerization was confirmed with data from neurons treated with latrunculin A. These neurons showed significantly decreased dextran uptake, compared to the ones treated with NMDA only. Additionally, adding latrunculin A to neurons also resulted in a significant decrease in CCP density. An explanation for this can be the loss of necessary binding sites present on F-actin for endocytic machinery to bind to (48). Interestingly, treating neurons with calpain inhibitor also resulted in significantly decreased CME and CCP density. The resulting effect elicited by the calpain inhibitor was even more pronounced compared to the effect of latrunculin A. This suggests that next to the role of NMDA in actin polymerization, calpain enzymes could also play an important role within this mechanism. This can be further supported by research showing that calpain activation increases with heightened activation of NMDA receptors (49-52). The decreased CCP density and CME suggest that calpain is a necessary factor in regulating endocytosis along the AIS. It could also be reasoned that calpain activity will enhance the stimulation of endocytosis even further by lowering membrane tension due to the cleavage of spectrins. However, the results are still preliminary and need more future studies. Based on the findings in this report and. Wernert, Moparthi *et al.*, the proposed mechanism for unlocking endocytosis along the AIS can be separated into two distinguishable layers; firstly, clearings with CCPs need to be formed within the spectrin mesh, and secondly, actin needs to polymerize around CCPs. Contrarily to the first layer, which is completely dependent on modulation of the spectrin mesh within the MPS, the second layer is found to be mostly independent of the MPS and its organization. This "ready-to-go" mechanism triggered by elevated neuronal activity such as LTD allows for stable protein assembly at the AIS.

Future perspectives – The proposed ready-to-go mechanism for CME along the AIS could potentially play an essential role in physiological processes of the brain such as axonal polarity, regulation of AIS length and plasticity. Because of the elevated neuronal activity during long-term potentiation (LTP) in memory consolidation, CME might even play an important part in this mechanism as well (53). At the same time, the MPS regulates CCP formation and forms a protective barrier under the axonal plasma membrane. The role of the MPS in CME could be studied further by using fluorogenic membrane lipids instead of using dextran feeding assays to visualize endocytic and endosomal activity at the membrane. Using technical optimization of MemGlow dyes by adding self-healing would be useful to study endocytosis during live cell imaging (54). Visualizing the membrane during live cell imaging would also be useful in studying the relationship between CME and the organization of actin rings within the MPS. We performed experiments in this direction where Memglow was compared to PK Mem, a fluorophore with self-healing properties due to integrated triplet-state quenchers in MemGlow dyes (54), for future use in live cell imaging (**supplementary figure 5**). Using confocal microscopy PK Mem

has been shown to reduce phototoxicity and enhance photostability (54), confirmed by our own live cell imaging experiments on a SoRa module (**supplementary figure 5**). The SoRa module concentrates the laser to a smaller area of the sample and exposes the dyes to an increased laser power compared to conventional confocal microscopy. A clear difference in photostability and phototoxicity was observable in the acquired microscopy images. Neurons stained with Memglow560 showed drastic morphology changes and blebbing after a short period of laser exposure, while PK Mem-treated neurons kept their morphology for a significantly longer period. Furthermore, PK Mem dyes bleached much slower compared to the Memglow560 dyes. For example, when using 10% laser power for 10 minutes with 600 frames 50% intensity was lost at frame 11 when stained for Memglow560 and at frame 600 when stained for PK Mem.

Perturbation of the spectrin scaffold within the MPS or dysregulation of the 'ready-to-go' CME mechanism could also lay at the pathophysiological basis of neurodegenerative disorders, such as AD. It was already observed in AD that CME and endosomal uptake are dysregulated and are implicated in AD progression (55). For example, increased endocytosis in AD has been observed to stimulate the production of Aβ protein out of internalized amyloid precursor protein (APP) (56). Although these observations show strong evidence implying the importance of CME in disease formation, there is a lack of studies on dysregulated endocytosis specifically along the axon. Therefore, elucidating the effect of the MPS on CME is essential in understanding diseases in which the axon is primarily affected, suggesting that the actin-spectrin scaffold might be disturbed. Furthermore, several studies also indicate pathologically enhanced LTD in AD but whether there is a relationship with dysregulated CME is not studied yet (57, 58). Additionally, increased endocytosis in AD has been observed to stimulate the production of Aβ protein out of internalized amyloid precursor protein (APP) (56).
Dysregulated clathrin-mediated endocytosis can also be linked to abnormal AIS length and remodelling. Abnormal AIS have already been observed in several neurological disease models such as epilepsy, AD, amyotrophic lateral sclerosis, autism spectrum disorder, and Angelman syndrome which can potentially be related to degradation of the MPS resulting in aberrant clathrin-mediated endocytosis (59-63). To link the implication of the MPS and its role in regulating endocytosis to these pathological phenomena we can rely on induced pluripotent stem cells (iPSCs) in future studies.
Furthermore, it would be interesting to continue exploring the effect of calpain on CCP formation and CME based on the obtained preliminary results. Experiments would include neurons treated with calpain inhibitor alone to compare the effect to neurons treated with both NMDA and calpain. The study of the effect of calpain on the MPS and CME would give us more insight into neurological diseases or central nervous system injuries in which calpain excessively breaks down scaffolding proteins such as β4-spectrin (35).

CONCLUSION

It can be concluded that the AIS harbors stalled CCPs in clearings depleted of spectrin. Partial perturbation of β4-spectrin, an AIS-specific cytoskeleton component, is only partially perturbed by diamide or NMDA. Physiological stimulation with NMDA increased CME and revealed the second layer important for unlocking CME along the AIS by polymerizing actin around CCPs. These findings shed light on the relationship between the MPS, CCP formation, and CME along the AIS. This will be of interest to future research in several neurological diseases and therapy development.

REFERENCES

1. Sejnowski T, Delbruck T. The language of the brain. Sci Am. 2012;307(4):54-9.
2. Salvadores N, Sanhueza M, Manque P, Court FA. Axonal Degeneration during Aging and Its Functional Role in Neurodegenerative Disorders. Front Neurosci. 2017;11:451.
3. Leterrier C, Potier J, Caillol G, Debarnot C, Rueda Boroni F, Dargent B. Nanoscale Architecture of the Axon Initial Segment Reveals an Organized and Robust Scaffold. Cell Rep. 2015;13(12):2781-93.
4. Rasband MN. The axon initial segment and the maintenance of neuronal polarity. Nat Rev Neurosci. 2010;11(8):552-62.
5. Huang CY, Rasband MN. Axon initial segments: structure, function, and disease. Ann N Y Acad Sci. 2018;1420(1):46-61.
6. Galiano MR, Jha S, Ho TS, Zhang C, Ogawa Y, Chang KJ, et al. A distal axonal cytoskeleton forms an intra-axonal boundary that controls axon initial segment assembly. Cell. 2012;149(5):1125-39.
7. Xu K, Zhong G, Zhuang X. Actin, spectrin, and associated proteins form a periodic cytoskeletal structure in axons. Science. 2013;339(6118):452-6.
8. Leterrier C. Putting the axonal periodic scaffold in order. Curr Opin Neurobiol. 2021;69:33-40.
9. Leterrier C. The Axon Initial Segment: An Updated Viewpoint. J Neurosci. 2018;38(9):2135-45.
10. Unsain N, Bordenave MD, Martinez GF, Jalil S, von Bilderling C, Barabas FM, et al. Remodeling of the Actin/Spectrin Membrane-associated Periodic Skeleton, Growth Cone Collapse and F-Actin Decrease during Axonal Degeneration. Sci Rep. 2018;8(1):3007.
11. Wernert F, Moparthi S, Lainé J, Moulay G, Boroni-Rueda F, Pelletier F, et al. The actin-spectrin submembrane scaffold restricts endocytosis along proximal axons. bioRxiv. 2023:2023.12.19.572337.
12. Mettlen M, Chen PH, Srinivasan S, Danuser G, Schmid SL. Regulation of Clathrin-Mediated Endocytosis. Annu Rev Biochem. 2018;87:871-96.
13. Roth TF, Porter KR. YOLK PROTEIN UPTAKE IN THE OOCYTE OF THE MOSQUITO AEDES AEGYPTI. L. J Cell Biol. 1964;20(2):313-32.
14. Lampe M, Vassilopoulos S, Merrifield C. Clathrin coated pits, plaques and adhesion. J Struct Biol. 2016;196(1):48-56.
15. Giani M, den Otter WK, Briels WJ. Clathrin Assembly Regulated by Adaptor Proteins in Coarse-Grained Models. Biophys J. 2016;111(1):222-35.
16. Willy NM, Ferguson JP, Akatay A, Huber S, Djakbarova U, Silahli S, et al. De novo endocytic clathrin coats develop curvature at early stages of their formation. Developmental Cell. 2021;56(22):3146-59.e5.
17. Bingham D, Wernert F, Moura JDC, Boroni-Rueda F, Bommel Nv, Caillol G, et al. Distinct nano-structures support a multifunctional role of actin at presynapses. bioRxiv. 2022:2022.05.18.492480.
18. Itofusa R, Tojima T, Kamiguchi H. Visualization of Clathrin-Mediated Endocytosis During Semaphorin-Guided Axonal Growth. Methods Mol Biol. 2017;1493:287-98.
19. Mann F, Miranda E, Weinl C, Harmer E, Holt CE. B-type Eph receptors and ephrins induce growth cone collapse through distinct intracellular pathways. J Neurobiol. 2003;57(3):323-36.
20. Tojima T, Itofusa R, Kamiguchi H. Asymmetric clathrin-mediated endocytosis drives repulsive growth cone guidance. Neuron. 2010;66(3):370-7.

21. Hines JH, Abu-Rub M, Henley JR. Asymmetric endocytosis and remodeling of beta1-integrin adhesions during growth cone chemorepulsion by MAG. Nat Neurosci. 2010;13(7):829-37.
22. Eichel K, Uenaka T, Belapurkar V, Lu R, Cheng S, Pak JS, et al. Endocytosis in the axon initial segment maintains neuronal polarity. Nature. 2022;609(7925):128-35.
23. Fréal A, Jamann N, Ten Bos J, Jansen J, Petersen N, Ligthart T, et al. Sodium channel endocytosis drives axon initial segment plasticity. Sci Adv. 2023;9(37):eadf3885.
24. Kaech S, Banker G. Culturing hippocampal neurons. Nat Protoc. 2006;1(5):2406-15.
25. Stil A, Liberelle B, Guadarrama Bello D, Lacomme L, Arpin L, Parent P, et al. A simple method for poly-D-lysine coating to enhance adhesion and maturation of primary cortical neuron cultures in vitro. Front Cell Neurosci. 2023;17:1212097.
26. Leyton-Puig D, Kedziora KM, Isogai T, van den Broek B, Jalink K, Innocenti M. PFA fixation enables artifact-free super-resolution imaging of the actin cytoskeleton and associated proteins. Biol Open. 2016;5(7):1001-9.
27. Jimenez A, Friedl K, Leterrier C. About samples, giving examples: Optimized Single Molecule Localization Microscopy. Methods. 2020;174:100-14.
28. Schmidt U, Weigert M, Broaddus C, Myers G, editors. Cell Detection with Star-Convex Polygons. Medical Image Computing and Computer Assisted Intervention – MICCAI 2018; 2018 2018//; Cham: Springer International Publishing.
29. Vangindertael J, Camacho R, Sempels W, Mizuno H, Dedecker P, Janssen KPF. An introduction to optical super-resolution microscopy for the adventurous biologist. Methods Appl Fluoresc. 2018;6(2):022003.
30. Sochacki KA, Shtengel G, van Engelenburg SB, Hess HF, Taraska JW. Correlative super-resolution fluorescence and metal-replica transmission electron microscopy. Nat Methods. 2014;11(3):305-8.
31. Wu XT, Sun LW, Yang X, Ding D, Han D, Fan YB. The potential role of spectrin network in the mechanotransduction of MLO-Y4 osteocytes. Sci Rep. 2017;7:40940.
32. Becker PS, Cohen CM, Lux SE. The effect of mild diamide oxidation on the structure and function of human erythrocyte spectrin. J Biol Chem. 1986;261(10):4620-8.
33. Lee HK, Kameyama K, Huganir RL, Bear MF. NMDA induces long-term synaptic depression and dephosphorylation of the GluR1 subunit of AMPA receptors in hippocampus. Neuron. 1998;21(5):1151-62.
34. Fujiwara I, Zweifel ME, Courtemanche N, Pollard TD. Latrunculin A Accelerates Actin Filament Depolymerization in Addition to Sequestering Actin Monomers. Curr Biol. 2018;28(19):3183-92.e2.
35. Schafer DP, Jha S, Liu F, Akella T, McCullough LD, Rasband MN. Disruption of the axon initial segment cytoskeleton is a new mechanism for neuronal injury. J Neurosci. 2009;29(42):13242-54.
36. Hu RJ, Bennett V. In vitro proteolysis of brain spectrin by calpain I inhibits association of spectrin with ankyrin-independent membrane binding site(s). J Biol Chem. 1991;266(27):18200-5.
37. Bahr BA, Tiriveedhi S, Park GY, Lynch G. Induction of calpain-mediated spectrin fragments by pathogenic treatments in long-term hippocampal slices. J Pharmacol Exp Ther. 1995;273(2):902-8.
38. Jenkins PM, He M, Bennett V. Dynamic spectrin/ankyrin-G microdomains promote lateral membrane assembly by opposing endocytosis. Sci Adv. 2015;1(8):e1500301.
39. Ghisleni A, Galli C, Monzo P, Ascione F, Fardin MA, Scita G, et al. Complementary mesoscale dynamics of spectrin and acto-myosin shape membrane territories during mechanoresponse. Nat Commun. 2020;11(1):5108.

40. Lorenzo DN. Cargo hold and delivery: Ankyrins, spectrins, and their functional patterning of neurons. Cytoskeleton (Hoboken). 2020;77(3-4):129-48.
41. Posor Y, Jang W, Haucke V. Phosphoinositides as membrane organizers. Nat Rev Mol Cell Biol. 2022;23(12):797-816.
42. Wu XS, Elias S, Liu H, Heureaux J, Wen PJ, Liu AP, et al. Membrane Tension Inhibits Rapid and Slow Endocytosis in Secretory Cells. Biophys J. 2017;113(11):2406-14.
43. Djakbarova U, Madraki Y, Chan ET, Kural C. Dynamic interplay between cell membrane tension and clathrin-mediated endocytosis. Biol Cell. 2021;113(8):344-73.
44. Krieg M, Dunn AR, Goodman MB. Mechanical control of the sense of touch by β-spectrin. Nat Cell Biol. 2014;16(3):224-33.
45. Collot M, Ashokkumar P, Anton H, Boutant E, Faklaris O, Galli T, et al. MemBright: A Family of Fluorescent Membrane Probes for Advanced Cellular Imaging and Neuroscience. Cell Chem Biol. 2019;26(4):600-14.e7.
46. Cooney JR, Hurlburt JL, Selig DK, Harris KM, Fiala JC. Endosomal compartments serve multiple hippocampal dendritic spines from a widespread rather than a local store of recycling membrane. J Neurosci. 2002;22(6):2215-24.
47. Yang C, Colosi P, Hugelier S, Zabezhinsky D, Lakadamyali M, Svitkina T. Actin polymerization promotes invagination of flat clathrin-coated lattices in mammalian cells by pushing at lattice edges. Nat Commun. 2022;13(1):6127.
48. Loebrich S. The role of F-actin in modulating Clathrin-mediated endocytosis: Lessons from neurons in health and neuropsychiatric disorder. Commun Integr Biol. 2014;7:e28740.
49. Gafni J, Ellerby LM. Calpain activation in Huntington's disease. J Neurosci. 2002;22(12):4842-9.
50. Andres AL, Regev L, Phi L, Seese RR, Chen Y, Gall CM, et al. NMDA receptor activation and calpain contribute to disruption of dendritic spines by the stress neuropeptide CRH. J Neurosci. 2013;33(43):16945-60.
51. Abe K, Takeichi M. NMDA-receptor activation induces calpain-mediated beta-catenin cleavages for triggering gene expression. Neuron. 2007;53(3):387-97.
52. Glantz SB, Cianci CD, Iyer R, Pradhan D, Wang KK, Morrow JS. Sequential degradation of alphaII and betaII spectrin by calpain in glutamate or maitotoxin-stimulated cells. Biochemistry. 2007;46(2):502-13.
53. Popik B, Crestani AP, Silva MO, Quillfeldt JA, de Oliveira Alvares L. Calpain modulates fear memory consolidation, retrieval and reconsolidation in the hippocampus. Neurobiol Learn Mem. 2018;151:53-8.
54. Ling J, Liu Y, Fu Y, Liu S, Ding L, Huang L, et al. A gentle palette of plasma membrane dyes. bioRxiv. 2024:2024.05.04.592408.
55. Zadka Ł, Sochocka M, Hachiya N, Chojdak-Łukasiewicz J, Dzięgiel P, Piasecki E, et al. Endocytosis and Alzheimer's disease. GeroScience. 2024;46(1):71-85.
56. Burrinha T, Gomes R, Terrasso AP, Almeida CG. Neuronal aging potentiates beta-amyloid generation via amyloid precursor protein endocytosis. bioRxiv. 2019:616540.
57. Tamagnini F, Burattini C, Casoli T, Balietti M, Fattoretti P, Aicardi G. Early impairment of long-term depression in the perirhinal cortex of a mouse model of Alzheimer's disease. Rejuvenation Res. 2012;15(2):231-4.
58. Taylor HBC, Emptage NJ, Jeans AF. Long-term depression links amyloid-β to the pathological hyperphosphorylation of tau. Cell Rep. 2021;36(9):109638.
59. Harty RC, Kim TH, Thomas EA, Cardamone L, Jones NC, Petrou S, et al. Axon initial segment structural plasticity in animal models of genetic and acquired epilepsy. Epilepsy Res. 2013;105(3):272-9.
60. Marin MA, Ziburkus J, Jankowsky J, Rasband MN. Amyloid-β plaques disrupt axon initial segments. Exp Neurol. 2016;281:93-8.

61. Usui N, Tian X, Harigai W, Togawa S, Utsunomiya R, Doi T, et al. Length impairments of the axon initial segment in rodent models of attention-deficit hyperactivity disorder and autism spectrum disorder. Neurochem Int. 2022;153:105273.
62. Kaphzan H, Buffington SA, Jung JI, Rasband MN, Klann E. Alterations in intrinsic membrane properties and the axon initial segment in a mouse model of Angelman syndrome. J Neurosci. 2011;31(48):17637-48.
63. Harley P, Kerins C, Gatt A, Neves G, Riccio F, Machado CB, et al. Aberrant axon initial segment plasticity and intrinsic excitability of ALS hiPSC motor neurons. Cell Rep. 2023;42(12):113509.

Acknowledgements – During my internship I was very grateful to work with highly skilled scientists and lab technicians, who supported me along the way. Therefore, I would like to thank Dr. Christophe Leterrier to give me the amazing and unique opportunity to realize my internship in the NeuroCyto lab at the Institute of Neurophysiopathology (INP). I would also like to thank him for his mentorship and the several learning opportunities that I had in his laboratory. Being in his laboratory made me develop a strong passion for microscopy. I would also like to thank Dr. Christophe Leterrier for involving me in the revision of Wernert, Moparthi *et al.* regarding the role of the MPS in endocytosis along proximal axons. It was a unique experience to be able to collaborate with the team in a publishing context.
I would also like to thank Florence Pelletier for teaching me valuable laboratory skills and scientific rigorousness and supporting me throughout my learning process. I could not have wished for a better mentor to teach me how to carry out the experiments. Additionally, I would like to thank Dr. Florian Wernert to share his knowledge with me on my project. I would also like to thank Fanny Boroni-Rueda for always providing me with neuronal cultures.
Furthermore, I would also like to thank Sofia Tumminia, Ciarán Butler-Hallissey, Christopher Parperis, Theresa Wiesner, and Louisa Mezache for the never-ending support and the shared laughs. Additionally, I would like to thank them for answering all my microscopy-related questions and assisting me on the microscope whenever I needed guidance. I am very grateful and proud that I got to complete my internship surrounded by wonderful people in the heart of Marseille.

Author contributions – Dr. Christophe Leterrier conceived and designed the research. Eline Simons and Florence Pelletier performed experiments. Eline Simons and Dr. Florian Wernert performed data analysis. Fanny Boroni-Rueda prepared the neuronal cultures. Eline Simons wrote the paper. All authors carefully edited the manuscript.

SUPPLEMENTARY RESULTS

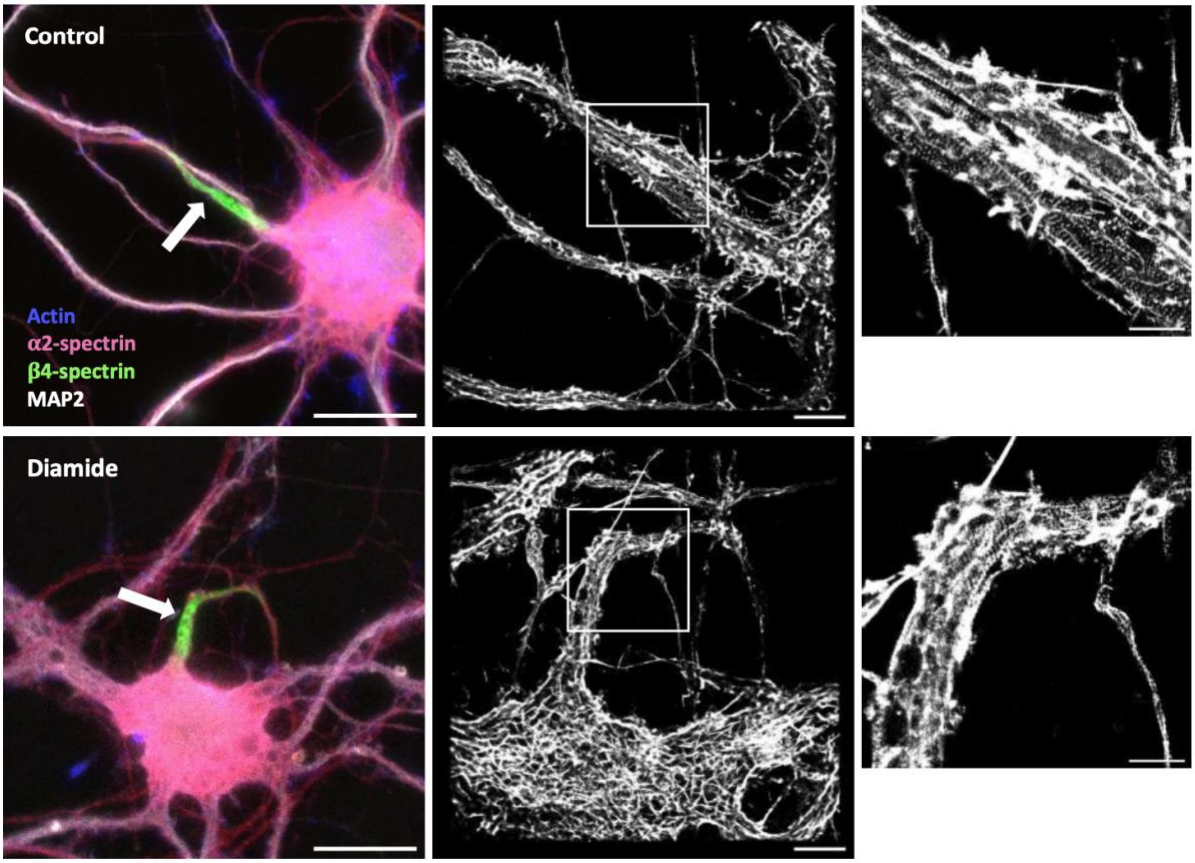

Supplementary 1: Diamide-treated hippocampal neurons seem to maintain actin periodicity at the AIS.

A-C. STORM images of cultured hippocampal neurons at DIV14 fixed and stained for actin with phalloidin (AttoPh647+). Neurons were treated with control (0,1% DMSO) or diamide (5 mM for 45 minutes). Images at the right are zooms corresponding to the white boxes of the center images (periodicity is difficult to observe). Arrows indicate the AIS. Scale bars; 20 µm (left images), 5 µm (center images), 2 µm (right images).

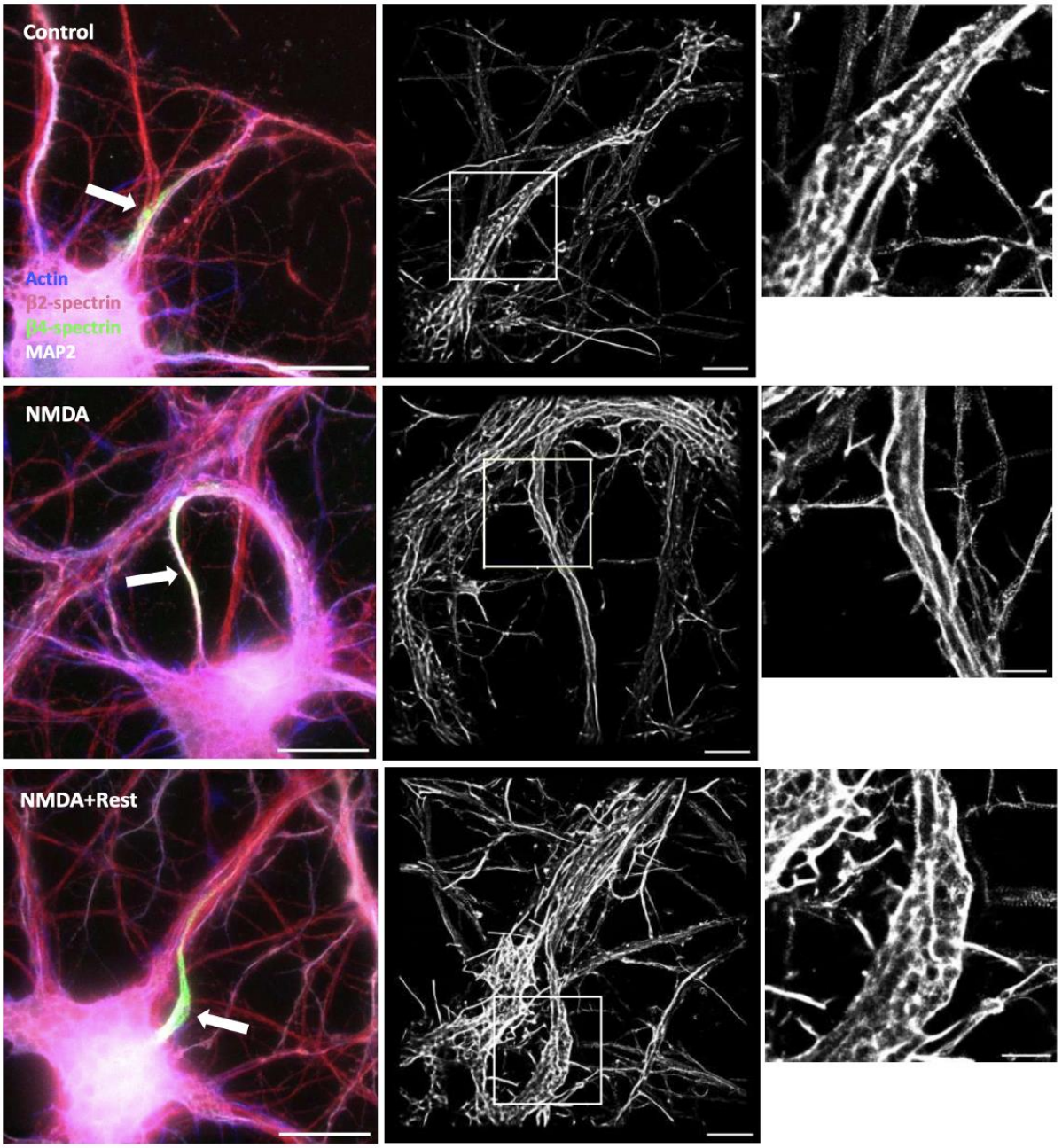

Supplementary figure 2: Absent actin periodicity after treatment in NB+ in the AIS of NMDA-treated hippocampal neurons.

A-C. STORM images of cultured hippocampal neurons at DIV15 fixed and stained for actin with phalloidin (AttoPh647+). Neurons were treated with control (uncomplemented NB) or NMDA (50 µM for 4 minutes). Images at the right are zooms corresponding to the white boxes of the center images (periodicity is difficult to observe). Scale bars; 20 µm (left images), 5 µm (center images), 2 µm (right images).

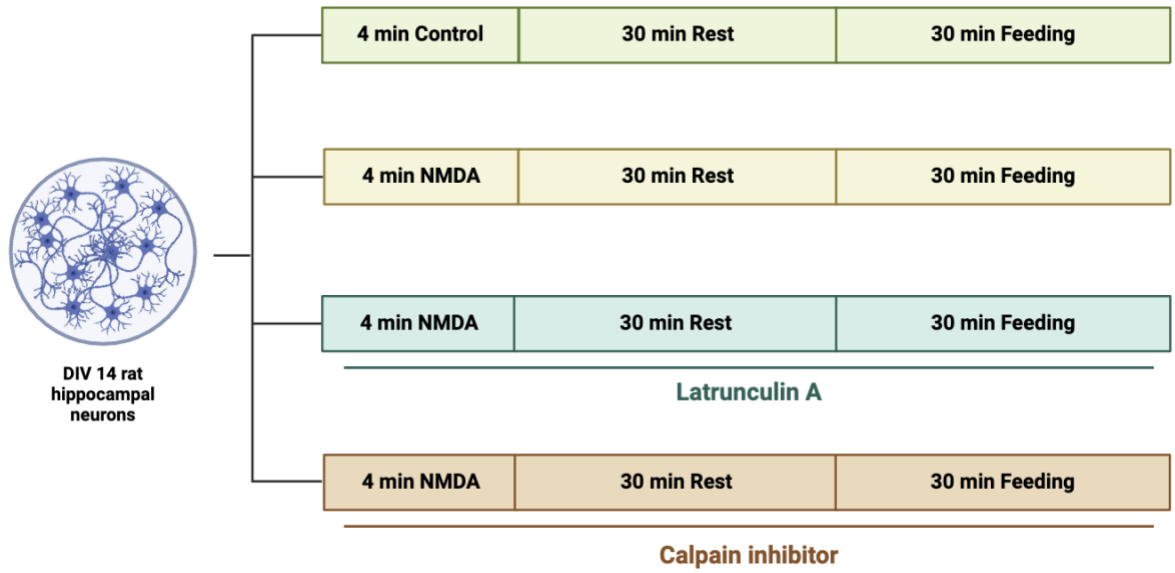

Supplementary figure 3: Schematic representation of the experimental setup of the dextran uptake assays in four different conditions.

Schematic visualization of the experimental setup. Four conditions in total were included in the experiment: control (uncomplemented NB), NMDA, NMDA+latranculin A, NMDA+calpain inhibitor. Figure made with Biorender.

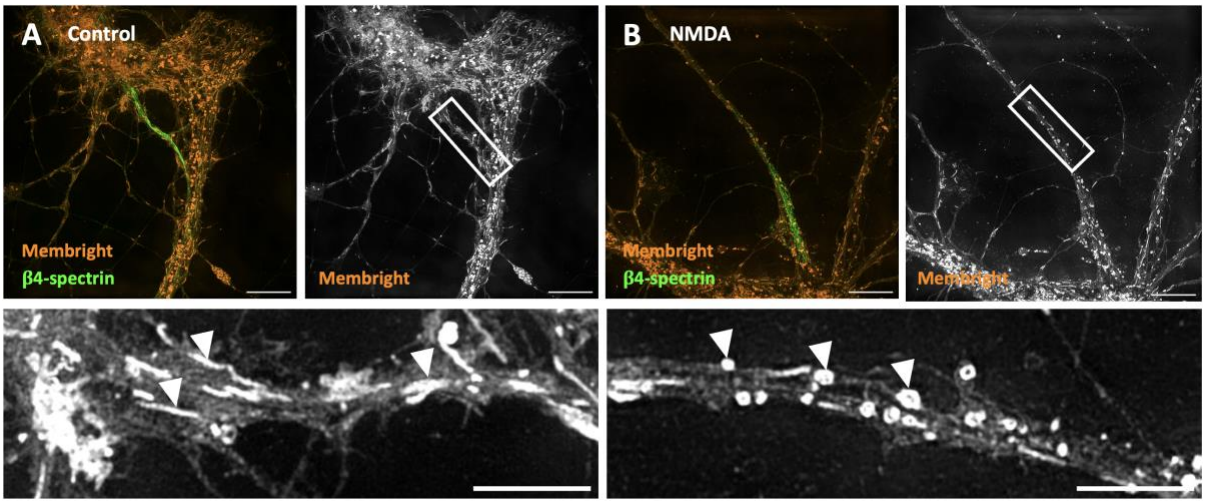

Supplementary figure 4: Elevated neuronal activity stimulates the formation of endosomal compartments along the AIS.

A-B. SIM images of cultured hippocampal neurons at DIV15 fixed and stained for β4-spectrin (AIS-specific). Memglow560 (200 nM for 30 min) was added to the experiment to show internalization of extracellular components. Neurons were treated with control (uncomplemented NB) or NMDA (50 µM for 4 minutes). Overlay of β4-spectrin and Memglow560 (top left image), single-color image of Memglow560 (top right image), zoom of the AIS corresponding to the white box in the top right image (bottom image). Arrowheads in the bottom images indicate tubular structures and endosomal compartments. Scale bars; 10 µm (top left images), 10 (top right images), 4 µm (bottom images).

A)

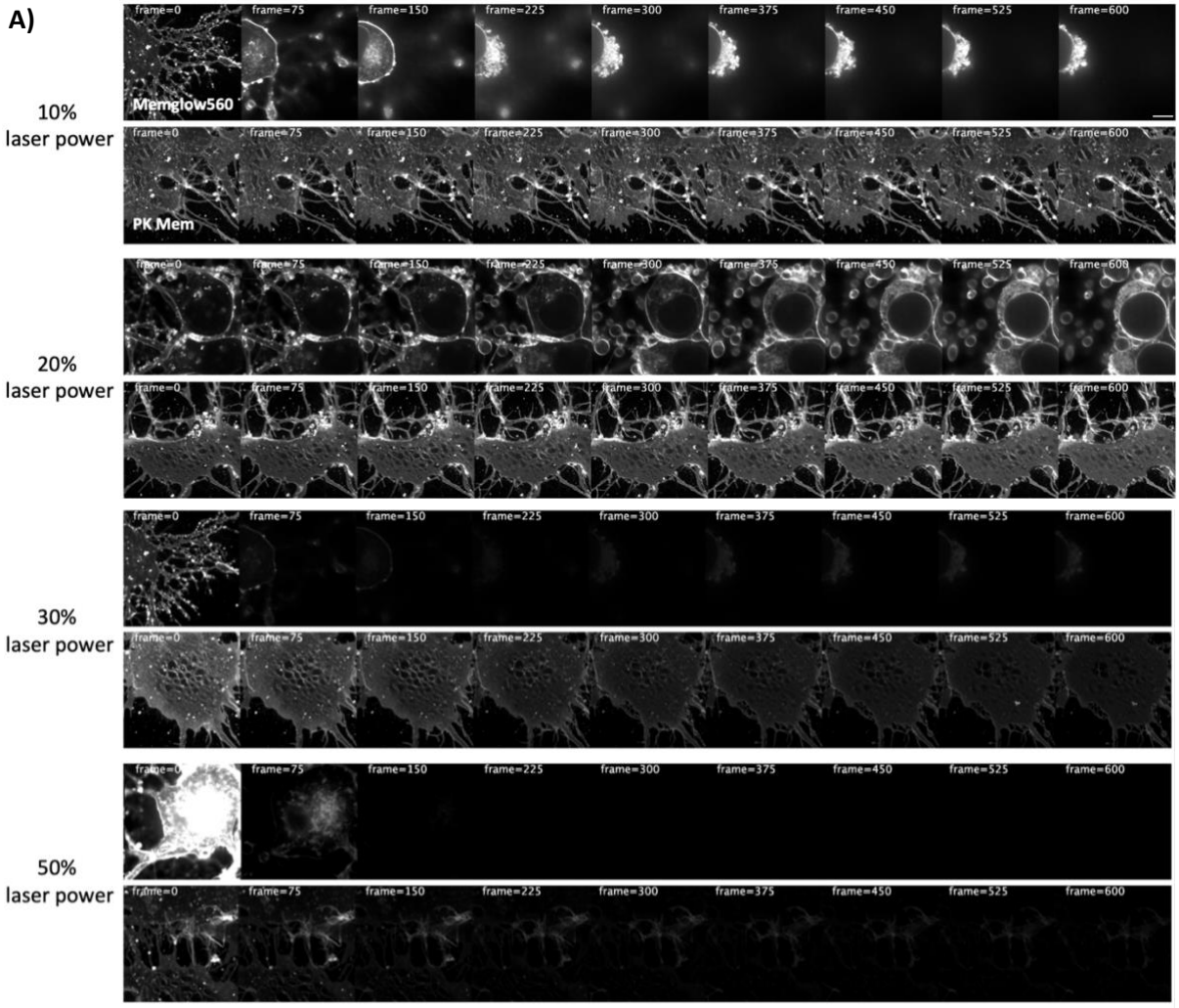
10% laser power
20% laser power
30% laser power
50% laser power
Memglow560
PK Mem
frame=0
frame=75
frame=150
frame=225
frame=300
frame=375
frame=450
frame=525
frame=600

B)

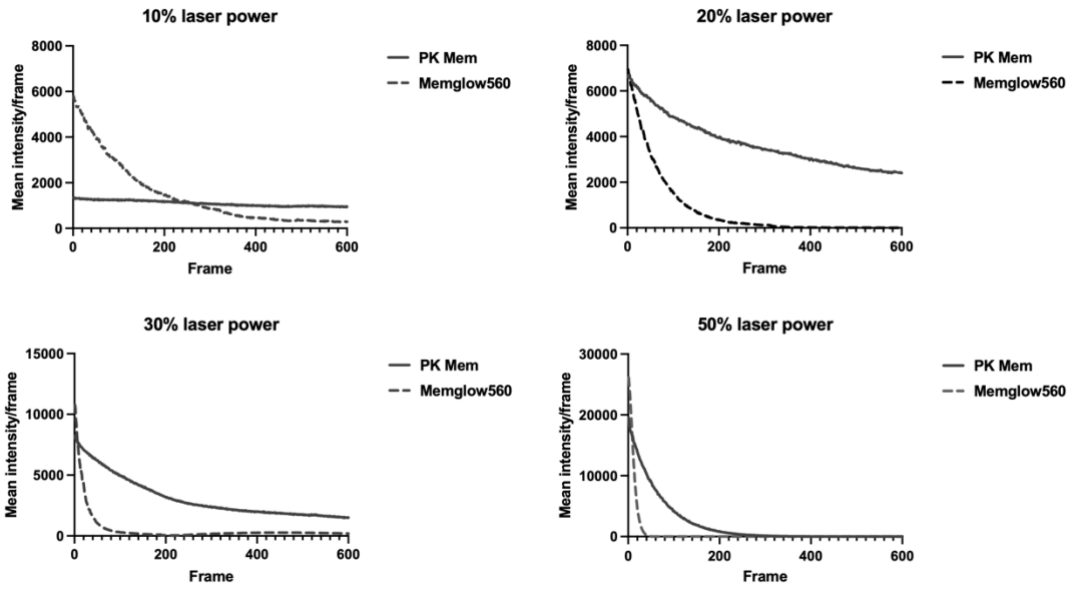
10% laser power
20% laser power
30% laser power
50% laser power
Mean intensity/frame
Frame
PK Mem
Memglow560

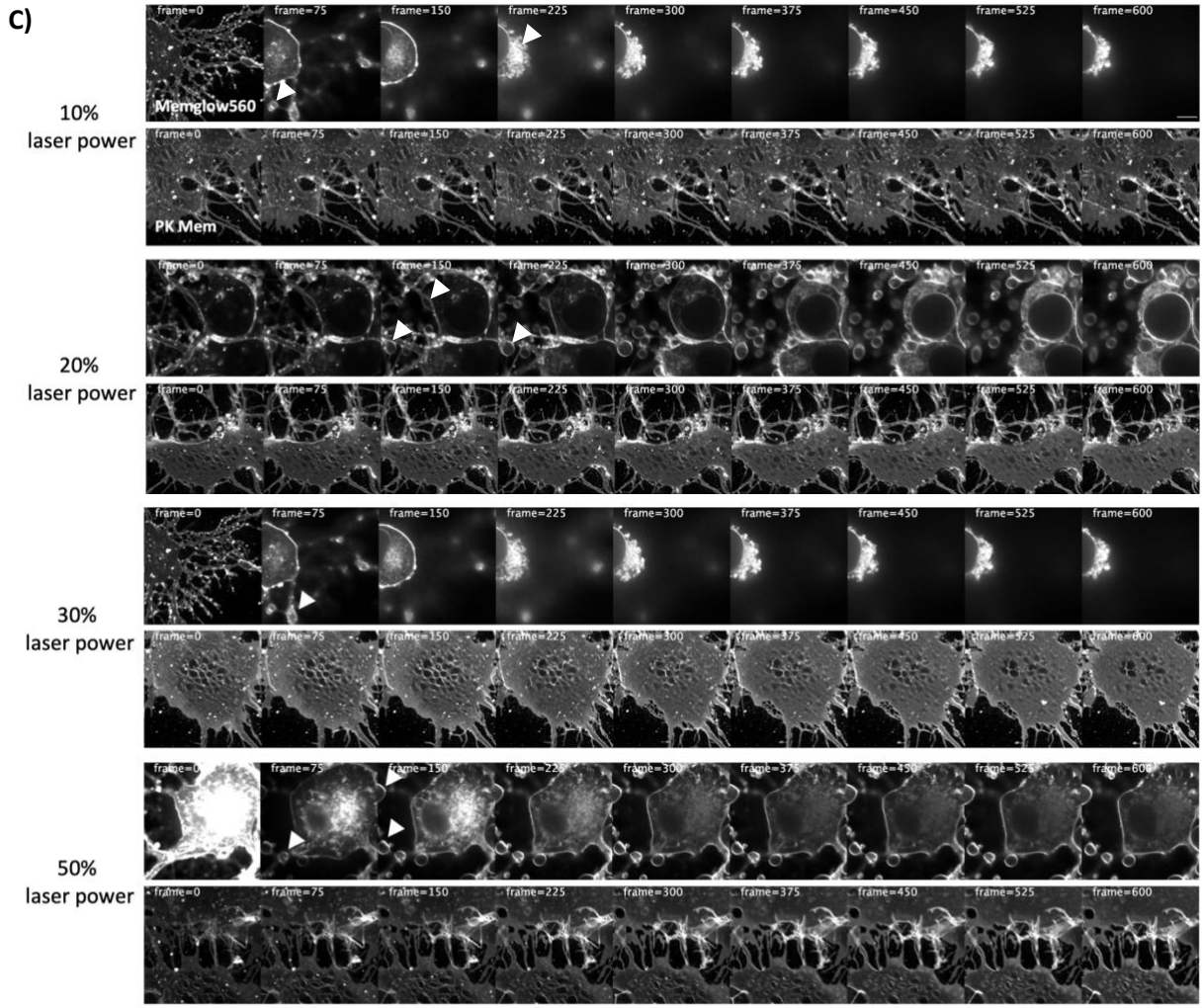

Supplementary figure 5: Staining neuronal membranes with a self-healing fluorophore enhances photostability and reduces cell phototoxicity.

Live cell images of cultured hippocampal neurons at DIV2 stained with Memglow560 (100 nM, no self-healing properties, upper images) or PK Mem 560 (100 nM, self-healing properties, lower images) to compare photostability and cell phototoxicity of the two fluorogenic membrane lipids. Images were acquired at 200 ms exposure time every 1 second for 10 minutes. Different laser power intensities were used for every recording (10%, 20%, 30%, 50%). **A.** Live cell images of cultured hippocampal neurons at DIV2 comparing photostability Memglow560 of PK Mem 560. **B.** Graphs comparing the decline in mean intensity/frame of Memglow560 stained neurons versus PK Mem stained neurons at different laser power intensities (10%, 20%, 30%, 50%). **C.** Same images as in A, but adjusted for contrast showing the phototoxic effect on stained neurons. White arrowheads indicate blebbing due to phototoxicity. Scale bar = 5 µm.